Advances in Nano Research, *Vol. 17, No.3 (2024) 257-274*
https://doi.org/10.12989/anr.2024.17.3.257

Dynamic response of FG carbon nanotubes nanoplates embedded in elastic media under moving point load

Mohamed A Eltaher*[1], Ismail Esen[2], Alaa A. Abdelrahman[3] and Azza M. Abdraboh[4]

[1]*Mechanical Engineering Department, Faculty of Engineering, King Abdulaziz University, P.O. Box 80204, Jeddah, Saudi Arabia*
[2]*Department of Mechanical Engineering, Karabuk University, Karabuk, Turkey*
[3]*Mechanical Design & Production Department, Faculty of Engineering, Zagazig University, P.O. Box 44519, Zagazig, Egypt*
[4]*Physics Department, Faculty of Science, Benha University, Benha, Egypt*

(*Received December 30, 2021, Revised September 4, 2024, Accepted September 10, 2024*)

Abstract. This work aims to study and analyse the dynamic size dependent behvior of functionally graded carbon nanotubes (FGCNTs) nanoplates embedded in elastic media and subjected to moving point load. The non-classical effect is incorporated into the governing equations using the nonlocal strain gradient theory (NSGT). Four different reinforcement configurations of the carbon nanotubes (CNTs) are considered to show the effect of reinforcement configuration on the dynamic behvior of the FGCNTs nanoplates. The material characteristics of the functionally graded materials are assumed to be continuously distributed throughout the thickness direction according to the power law. The Hamiltonian principle is exploited to derive the dynamic governing equations of motion and the associated boundary conditions in the framework of the first order shear deformation plate theory. The Navier analytical approach is adopted to solve the governing equations of motion. The obtained solution is checked by comparing the obtained results with the available results in the literature and the comparison shows good agreement. Numerical results are obtained and discussed. Obtained results showed the significant impact of the elastic foundation parameters, the non-classical material parameters, the CNT configurations, and the volume fractions on the free and forced vibration behaviors of the FGCNT nanoplate embedded in two parameters elastic foundation and subjected to moving load.
Keywords: FGCNTs nanoplate; elastic media; moving point load; non-classical effect; NSGT; reinforcement configuration

1. Introduction

Due to their high stiffness to weight ratio and strength to weight ratio, the multi-layered composite structures are broadly employed in different real applications such as airplanes, torpedoes, space craft structures etc. To enhance mechanical, electrical, and thermal properties of composite structures, carbon nanotubes (CNTs) are anticipated and utilized as an alternative to the conventional fibers due to their outstanding characteristics. Functionally Graded Carbon Nanotubes (FGCNTs) nanostructures are considered as a new class of composite materials and have received great attention from scientists due to their distinguishing characteristics. FGCNTs have numerous appealing characteristics including the ability to control deformation, resistance, and dynamic response, as well as minimize or eliminate stress concentrations, smooth thermal stress transitions, and boost oxidation resistance, are all advantages. This class of modern nanocomposites has been widely used in a variety of industrial and mechanical applications, such as nuclear reactor components, aerospace, energy conversion, turbine blade, engine components, automotive, optics, chemistry, bioengineering, microelectromechanical (MEMS) and nano-electronmechanical (NEMS) devices, (Eltaher *et al*. 2014, Daikh *et al*. 2020, She *et al*. 2021). Generally, functionally graded materials (FGMs) are made up of a combination of metals and ceramics, and they're distinguished by a smooth and continuous change in mechanical characteristics from one surface to the next, (She 2021). Carbon nanotubes are used as a reinforcement to enhance the mechanical characteristics of these modern composites. Because of its low thermal conductivity, ceramic resists high temperatures and protects metal from oxidation. The metal, on the other hand, is a ductile material that inhibits fracture induced by stresses caused by mechanical loads as well as high temperature gradients.

For nanobeam analyses, Arefi *et al*. (2018) exploited third-order shear deformation beam theory to study magneto-electro-thermoelastic of FG nonlocal nanobeam subjected to magneto-electro-elastic loads. Abo-Bakr *et al*. (2020) evaluated the optimum weigh and gradation index of axially functionally graded Timoshenko microbeams under buckling and vibration constraint by using multiobjective particle swarm optimization, the Pareto optimal solutions, and modified couple stress theory. Daikh *et al*. (2020) studied static response of multilayer FG-CNTRC nonlocal strain gradient nanobeam using hyperbolic shear deformation theory. Mahesh and Harursampath (2020) addressed the nonlinear deflection problem of magneto-electro-elastic shells reinforced with carbon nanotubes subjected to multi-physics loads by using finite element method. Jena *et al* (2020) presented effects of surface energy and surface residual stresses on vibro-thermal response of chiral, zigzag, and armchair types of SWCNTs using refined beam

*Corresponding author, Professor,
E-mail: meltaher@kau.edu.sa

ISSN: 2287-237X (Print), 2287-2388 (Online)

theory. Alazwari *et al*. (2021) examined a buckling of cross-ply multilayered nonlocal strain gradient nanobeams reinforced by carbon nanotube by using a novel hyperbolic higher shear deformation theory including thickness stretching effect. Babaei *et al*. (2021) exploited Biot poroelastic law instead of Hooke's law is used to study the vibration response of FG porous rotating thick truncated cone. Daikh *et al*. (2021a) studied buckling of cross-ply FG-CNTRC curved sandwich nonlocal strain gradient nanobeams in thermal environment based on a novel quasi-3D higher-order shear deformation theory. Esen *et al*. (2021a, b) investigated the natural frequencies and buckling stability of a cracked and uncracked FG microbeam embedded in an elastic matrix and exposed to magnetic field in a thermal environment based on nonlocal elasticity and nonlocal strain gradient theories.

For nanaplate analyses, Barati (2017) studied forced vibration of nonlocal-strain gradient of metal foam nanoplates with uniform and graded porosities. Ebrahimi *et al*. (2019) presented hygro-thermal effects on wave dispersion responses of magnetostrictive sandwich nanoplates rested on elastic foundation. Dehshahri *et al*. (2020) investigated the free vibrations of the modified strain gradient theory nanoplates made 3D-FGM. Esmaeilzadeh *et al*. (2020) revealed the dynamic response of 2D FG porous nanoplates resting on Winkler and Pasternak elastic foundations. Kachapi (2020) studied pull-in instability and nonlinear vibration of fluid-conveying piezoelectric nanosensor subjected to nonlinear electrostatic and harmonic excitations and viscoelastic foundation using Gurtin-Murdoch surface/ interface theory. Kolahdouzan *et al*. (2020) investigated free vibration and buckling analysis of elastically restrained FGCNTRC sandwich annular nanoplates via layer-wise theory. Radwan and Sobhy (2020) analysed transient instability of viscoelastic sandwich CNTs-reinforced microplates exposed to 2D magnetic field and hygrothermal conditions. Analooei *et al*. (2021) investigated the thermo-electro-mechanical static and dynamic stability nonlocal nanoplates with B3-spline finite strip method. Daikh *et al*. (2021b) derived analytical solutions for bending and buckling responses of axially temperature-dependent FG-CNTRC plate based on higher order shear deformation theory. Daikh *et al*. (2021c) developed a novel nonlocal strain gradient Quasi-3D model to examine bending behaviour of sigmoid FG sandwich nanoplates. Farahmand (2021) studied buckling solution of two-variable refined plate moderately thick strain gradient theory microplate. Habibi *et al*. (2021) studied buckling and vibrational characteristics of a porous composite cylindrical nanoshell reinforced with graphene-reinforced composites. Liu *et al*. (2021) adopted the nonlocal strain gradient theory to reveal the vibration behaviour of laminated nanoplate with piezo-magnetic face sheets in its upper and lower surfaces. Pham *et al*. (2021) exploited a new third-order finite element method and nonlocal elasticity theory to explore the free vibration of nanoplates with auxetic honeycomb core using. Esmaeilzadeh *et al*. (2021) presented the geometrically nonlinear thermomechanical response of graphene-reinforced moving polymer nanoplates. Khadir *et al*. (2021) developed a novel four-unknowns quasi 3D theory to study bending, buckling and free vibration of FG carbon nanotubes reinforced composite laminated nanoplates. Bouafia *et al*. (2021) examined the natural frequencies of FGM nanoplates embedded in an elastic medium via nonlocal elasticity. Zhang *et al*. (2021) studied the effect of nanoscale surface energy parameters on the snap-buckling of FG-CNTR curved nanobeams. Lu *et al*. (2021) examined size-dependent postbuckling analysis of graphene reinforced composite microtubes with geometrical imperfection. Ding *et al*. (2021) developed a higher-order beam model to study the snap-buckling analysis of FG pipes conveying fluid.

Identifying and affecting the motion of nanoparticles are crucial for micro/nano-assembly, microfluidics, biological and colloidal science applications, chemical mechanical polishing, and xerographic processes, Eglin *et al*. (2006). Nanotubes are used to transport drug materials into targeted nano-sized molecules to change the behaviour of cancer cells, Roudbari *et al*. (2020). Therefore, understanding the mechanism of mass transport and the dynamic behaviour of microbeams under such loadings would be of great importance for the optimal design of beam-type micro-structures in the future, Şimşek (2010).

Qu *et al*. (2017) concerned with the numerical analysis of structural and acoustic behaviours of composite laminated plates under the action of moving loads. Şimşek and Aydın (2017) illustrated sizedependent influence in forced vibration of an imperfect FG modified couple stress microplate with porosities subjected to a moving load. Esen *et al*. (2020) developed a modified continuum finite element model to study the dynamic response of perforated modified couple microbeam under the effect of moving mass. Abdelrahman *et al*. (2021a, b) presented the influence perforation on the response of nonlocal strain gradient nanobeams under moving loads using analytical Navier methodology and numerical finite element method. Abdelrahman *et al*. (2021c) exploited a nonclassical size dependent model to examine the vibration response of CNTs reinforced composite beam resting on elastic foundations under a moving load. Assie *et al*. (2021) studied the dynamic vibration of 2D perforated thick beam under a moving load using finite element simulation and Newmark time integration method. Eltaher *et al*. (2021) predicted the dynamic response of nanoscale Timoshenko CNTs based on doublet mechanics under moving load. Esen *et al*. (2021c) studied dynamic response of nonlocal strain gradient FG-CNTRC nanobeam under moving point load in frame of Reddy beam theory. Esen *et al*. (2021d,e) exploited a size-dependent nonlocal strain gradient theory to examine the dynamic response of symmetric and sigmoid FG nanobeam and rested on elastic foundations by using numerical finite element simulation. Zhang *et al*. (2021) presented a novel computational approach to study a vibration of FG grapheneplatelet reinforced porous beams resting on a Winkler–Pasternak elastic foundation under a moving load. Rai and Gupta (2021) examined nonlinear vibrations of a polar-orthotropic thin circular plate subjected to circularly moving point load.

Based on the above shortlisted review previous work and according to authors' knowledge, analysis of the non-classical size dependent dynamic vibration response of FGCNT nanoplates resting on elastic media under a moving load hasn't been considered previously. Therefore, this

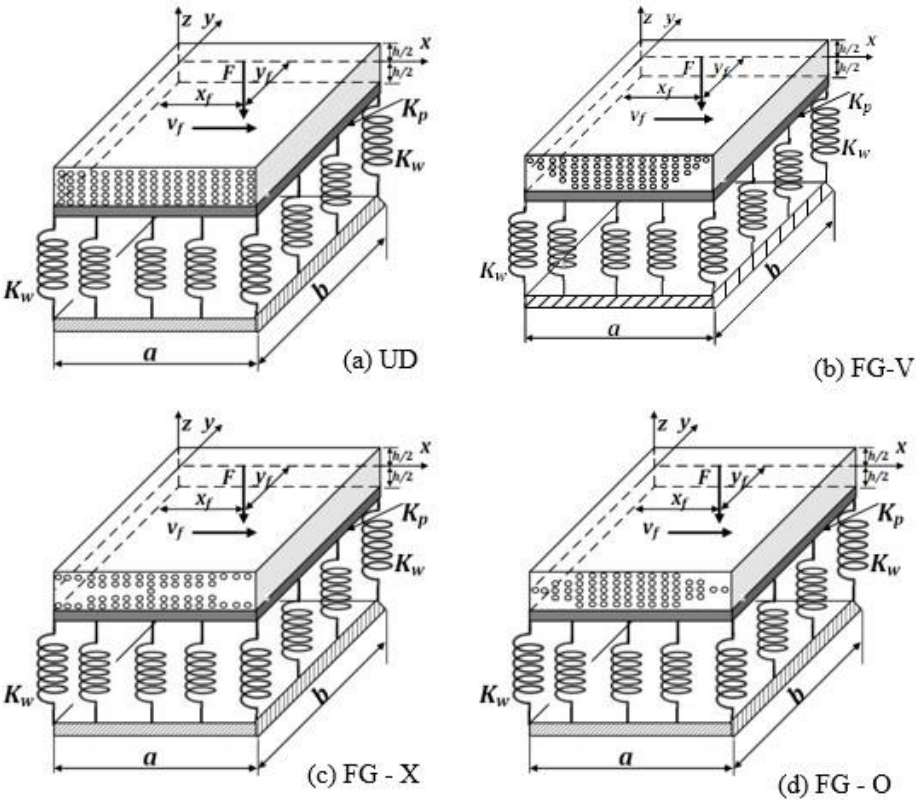

Fig. 1 The carbon nanotube functionally graded microplates with different configurations in the thickness direct ion along x axis on an elastic foundation

article aims to cover this topic and fill this gap by development a nonclassical size dependent model and solution procedure to comprehensively study and analyze the free as well as the forced vibration response of FGCNT nanoplate embedded in elastic media under moving load based on nonlocal strain gradient theory. The rest of the article is organized as follows: Section 2 will cover the mathematical formulations and modified constitutive stress-strain equations. Section 3 will present the analytical Navier solutions procedure for the governing equations of motion. Verifications with previous published works are presented and discussed in section 4. Numerical results and parametric analysis for free and forced vibration of FGCNT nanoplates are illustrated and deliberated in section 5. The revealed concluding remarks are summarized in section 6.

2. Mathematical formulation

Within this section the mathematical formulations including the effective properties of FG-CNT micro plates, kinematic relations, review of the nonlocal strain gradient theory, constitutive relations and finally the dynamic equations of motion with the associated boundary conditions of functionally graded CNT microplate embedded in an elastic media are presented.

2.1 Effective properties of FG-CNT micro plates

Consider the CNT microplate embedded in an elastic media with the following geometrical characteristics: length *a*, width *b*, thickness *h*, as shown in Fig. 1. Four types of aligned CNT reinforced plates are considered as shown in Fig. 1, namely uniformly distributed CNT beams (UD-CNT), functionally graded CNT beams type Λ (FGV-CNT) with densified CNT in the lower region, and functionally graded CNT beams type X (FGX-CNT) with the concentrated CNT in both the upper and lower regions. Functionally graded, TYPE O, (FGO-CNT) as shown in Fig. 1. The orientations of reinforcing CNT are along the length direction, which is the *x*-axis. It is assumed that all reinforced beams are in the same dimensions with the same total weight m_{TCNT} and volume fraction V_{TCNT} of CNTs, but in the V, X and O types, the distribution of the CNTs are according to a power law.

Thus, the distribution of the CNTs in FGV-CNT in the thickness direction is given by (Bouazza and Zenkour 2020, Shen 2009, Wattanasakulpong and Ungbhakorn 2013)

$$\mu(z) = \left(\frac{h+2z}{2h}\right)^{k}, \quad \left(-\frac{h}{2} \le z \le \frac{h}{2}\right) \tag{1}$$

And the corresponding volume fraction of CNTs is derived as

$$V_{CNT}(z) = (\Theta+1)\mu(z)V^{*}_{CNT}, \qquad \left(-\frac{h}{2} \le z \le \frac{h}{2}\right) \tag{2a}$$

with Θ refers to the nonlinearity distribution of the CNT shape function, Θ ≥ 1. However from the practical perspective, only linear distribution is considered in the current study, i.e., Θ = 1. According to linear distribution, Eq. (2) is rewritten as

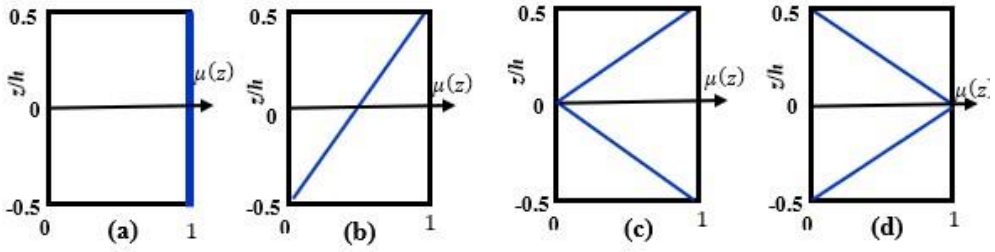

Fig. 2 CNT distribution shape function of FG-CNT plate; (a) UD (b) FG-V-type, (c) FG-X-type and (d) FG-O -type

$$V_{CNT}(z) = 2\mu(z)V^*_{CNT}, \quad \left(-\frac{h}{2} \le z \le \frac{h}{2}\right) \tag{2b}$$

For the considered CNT reinforced distributions, assume that they will have the same geometries and contain the same value of total weight of CNTs m_{TCNT}, and with total CNTs volume fraction $V_{CNT}{}^*$ (z) expressed as.

$$V^*_{CNT} = \frac{W_{CNT}}{W_{CNT} + \left(\frac{\rho_{CNT}}{\rho_m}\right)\{1 - W_{CNT}\}} \tag{2c}$$

and W_{CNT} represents CNT mass volume; ρ_m and ρ_{CNT} denote the matrix and CNT density parameters. For X type FGX-CNT the distribution and volume fraction of CNTs is (Lin and Xiang 2014)

$$\mu(z) = \left(\frac{2|z|}{h}\right)^k, \quad \left(-\frac{h}{2} \le z \le \frac{h}{2}\right) \tag{3}$$

$$V_{CNT}(z) = (k+1)\mu(z)V^*_{CNT}, \quad \left(-\frac{h}{2} \le z \le \frac{h}{2}\right) \tag{4}$$

For FGO the distribution and volume fraction (Thang *et al*. 2021)

$$\mu(z) = \left(1 - \frac{2|z|}{h}\right)^k, \quad \left(-\frac{h}{2} \le z \le \frac{h}{2}\right) \tag{5}$$

$$V_{CNT}(z) = (k+1)\mu(z)V^*_{CNT}, \quad \left(-\frac{h}{2} \le z \le \frac{h}{2}\right) \tag{6}$$

For UD-CNT beams the distribution are uniform along the thickness and the volume fraction of the CNTs is the same as the total volume fraction of the CNTs. Thus,

$$V_{CNT}(z) = V^*_{CNT}, \quad \left(-\frac{h}{2} \le z \le \frac{h}{2}\right). \tag{7}$$

The different orientation of reinforced CNT shape function distribution throughout the plate thickness are illustrated in Fig. 2 for linear distribution.

The effective material properties are evaluated from the results of molecular dynamics simulations (Griebel and Hamaekers 2004, Han and Elliott 2007) and a rule of mixture. The expressions of the properties are (Shen 2009).

$$E_{11}(z) = \eta_1 V_{CNT}(z)E^{cnt}_{11} + V_m(z)E^m, \tag{8a}$$

$$\begin{aligned} \frac{\eta_2}{E_{22}(z)} &= \frac{V_{CNT}(z)}{E^{cnt}_{22}} + \frac{V_m(z)}{E^m}, \\ \frac{\eta_3}{G_{12}(z)} &= \frac{V_{CNT}(z)}{G^{cnt}_{12}} + \frac{V_m(z)}{G^m}, \end{aligned} \tag{8b}$$

$$\begin{aligned} \upsilon_{12}(z) &= V_{CNT}(z)\upsilon^{cnt}_{12} + V_m(z)\upsilon^m, \\ \upsilon_{21}(z) &= \frac{\upsilon_{12}(z)}{E_{11}(z)}E_{22}(z), \end{aligned} \tag{8c}$$

$$\begin{aligned} \rho(z) &= V_{CNT}(z)\rho^{cnt} + V_m(z)\rho^m, \\ V_m(z) &= 1 - V_{CNT}(z) \end{aligned} \tag{8d}$$

Here, E^m, G^m, $E_{11}{}^{cnt}$, $E_{22}{}^{cnt}$, $G_{12}{}^{cnt}$ are Young's modulus and shear modulus of matrix and CNT, η_i , (i = 1, 2 and 3) are efficiency parameters of CNT/matrix; υ^m and $\upsilon_{12}{}^{cnt}$ are Poisson's ratios of matrix and CNT, and ρ^m and ρ^{cnt} are mass densities of matrix and CNT, respectively. The effective $E(z)$ and $G(z)$ are given by (Lin and Xiang 2014) as

$$E(z) = \frac{E_{11}(z)}{1 - \upsilon_{12}(z)\upsilon_{21}(z)}, \quad G(z) = G_{12}(z) \tag{9}$$

2.2 Kinematic and kinetic relations

In the context of the 1st order shear deformation theory (FSDT), the displacement field is given in the following form, (Reddy 1999, Pham *et al*. 2021):

$$\begin{Bmatrix} u(x,y,z,t) \\ v(x,y,z,t) \\ w(x,y,z,t) \end{Bmatrix} = \begin{bmatrix} 1 & 0 & 0 & z & 0 \\ 0 & 1 & 0 & 0 & z \\ 0 & 0 & 1 & 0 & 0 \end{bmatrix} \begin{bmatrix} u_0(x,y,t) \\ v_0(x,y,t) \\ w_0(x,y,t) \\ \phi_x(x,y,t) \\ \phi_y(x,y,t) \end{bmatrix} \tag{10}$$

Here, u, v and w denote the displacements and $u_0(x, y, t)$ $v_0(x, y, t)$ and $w(x, y, t)$ represent the mid-plane displacements in x, y and z axes respectively and $\phi_x(x, y, t)$ and $\phi_y(x, y, t)$ are the rotation of the cross-section . Based on the displacement field given in Eq. (10), the nonzero strain field components are expressed as (Reddy 1999)

$$\begin{Bmatrix} \varepsilon_{xx} \\ \varepsilon_{yy} \\ \gamma_{yz} \\ \gamma_{xz} \\ \gamma_{xy} \end{Bmatrix} = \begin{bmatrix} \frac{\partial}{\partial x} & 0 & 0 & z\frac{\partial}{\partial x} & 0 \\ 0 & \frac{\partial}{\partial y} & 0 & 0 & z\frac{\partial}{\partial y} \\ 0 & 0 & \frac{\partial}{\partial y} & 0 & 1 \\ 0 & 0 & \frac{\partial}{\partial x} & 1 & 0 \\ \frac{\partial}{\partial y} & \frac{\partial}{\partial x} & 0 & z\frac{\partial}{\partial y} & z\frac{\partial}{\partial x} \end{bmatrix} \begin{bmatrix} u_0(x,y,t) \\ v_0(x,y,t) \\ w_0(x,y,t) \\ \phi_x(x,y,t) \\ \phi_y(x,y,t) \end{bmatrix} \tag{11}$$

The material constitutive relationships can be expressed as follows

$$\begin{Bmatrix}\sigma_{xx}\\ \sigma_{yy}\\ \tau_{yz}\\ \tau_{xz}\\ \tau_{xy}\end{Bmatrix}=\begin{bmatrix}\frac{E_{11}(z)}{1-\upsilon_{12}(z)\upsilon_{21}(z)} & \frac{\upsilon_{12}(z)\,E_{22}(z)}{1-\upsilon_{12}(z)\upsilon_{21}(z)} & 0 & 0 & 0\\ \frac{\upsilon_{12}(z)\,E_{22}(z)}{1-\upsilon_{12}(z)\upsilon_{21}(z)} & \frac{E_{22}(z)}{1-\upsilon_{12}(z)\upsilon_{21}(z)} & 0 & 0 & 0\\ 0 & 0 & G_{23}(z) & 0 & 0\\ 0 & 0 & 0 & G_{13}(z) & 0\\ 0 & 0 & 0 & 0 & G_{12}(z)\end{bmatrix}\begin{Bmatrix}\varepsilon_{xx}\\ \varepsilon_{yy}\\ \gamma_{yz}\\ \gamma_{xz}\\ \gamma_{xy}\end{Bmatrix} \tag{12}$$

The force and moment resultants can be expressed as

$$\begin{Bmatrix}N_{xx}\\ N_{yy}\\ N_{xy}\end{Bmatrix}=\int_{-\frac{h}{2}}^{\frac{h}{2}}\begin{Bmatrix}\sigma_{xx}\\ \sigma_{yy}\\ \tau_{xy}\end{Bmatrix}dz,$$

$$\begin{Bmatrix}M_{xx}\\ M_{yy}\\ M_{xy}\end{Bmatrix}=\int_{-\frac{h}{2}}^{\frac{h}{2}}\begin{Bmatrix}\sigma_{xx}\\ \sigma_{yy}\\ \tau_{xy}\end{Bmatrix}zdz, \tag{13}$$

$$\begin{Bmatrix}Q_{xx}\\ Q_{yy}\end{Bmatrix}=\int_{-h/2}^{h/2}\begin{Bmatrix}\tau_{xz}\\ \tau_{yz}\end{Bmatrix}dz.$$

where N_{xx}, N_{yy} and N_{xy} are normal and shearing forces, M_{xx}, M_{yy} and M_{xy} are moments and Q_{xx} and Q_{yy} are transverse shearing forces.

2.3 Review of the nonlocal strain gradient theory

Based on the NSGT, the total stress tensor is expressed as (Lim *et al*. 2015):

$$t_{ij}=\sigma_{ij}-\nabla\sigma_{ij,m}^{(1)} \tag{14}$$

where ∇ denotes the Lapacian operator; σ_{ij} and $\sigma_{ij,m}^{(1)}$ refer to the corresponding stress and the higher order stress tensors; respectively. These stress tensors are given by the following relation:

$$\begin{Bmatrix}\sigma_{ij}\\ \sigma_{ijm}^{(1)}\end{Bmatrix}=\begin{Bmatrix}\int_{\Omega}\alpha_0(\boldsymbol{x}',\boldsymbol{x},e_0a)C_{ijkl}\varepsilon'_{kl}d\Omega'\\ l^2\int_{\Omega}\alpha_1(\boldsymbol{x}',\boldsymbol{x},e_1a)C_{ijkl}\varepsilon'_{kl,m}d\Omega'\end{Bmatrix} \tag{15}$$

where Ω refers to the bulk volume of the nanoplate, $e_0\ a$ and $e_1\ a$ represent two nonlocal parameters, l is also a characteristic length that has been introduced in Eq. (13) to account for the strain gradient elasticity effect. Herein, $\alpha_0(\boldsymbol{x}',\boldsymbol{x},e_0a)$ and $\alpha_1(\boldsymbol{x}',\boldsymbol{x},e_1a)$ represent two kernel parameters. Considering $e_0=e_1=e$ and (α_0, α_1) satisfy the corresponding condition reported in Eringen, (1983), the stress-strain relations have been introduced in (13) can be given by, (Thang *et al*. 2021)

$$(1-(ea)^2\nabla^2)\begin{Bmatrix}\sigma_{ij}\\ \sigma_{ijm}^{(1)}\end{Bmatrix}=\begin{Bmatrix}C_{ijkl}\,\varepsilon_{kl}\\ l^2C_{ijkl}\,\varepsilon_{kl,m}\end{Bmatrix} \tag{16}$$

According to Eq. (14), the total stress tensor can be cast in the following form:

$$(1-(ea)^2\nabla^2)t_{ij}=(1-l^2\nabla^2)C_{ijkl}\varepsilon_{kl} \tag{17}$$

Based on the NGST, the total normal and shear stress components are derived as (Lim *et al*. 2015)

$$(1-(ea)^2\nabla^2)\begin{Bmatrix}\sigma_{xx}^{(t)}\\ \sigma_{yy}^{(t)}\\ \tau_{yz}^{(t)}\\ \tau_{xz}^{(t)}\\ \tau_{xy}^{(t)}\end{Bmatrix}=[1-l_m^2\nabla^2]\begin{bmatrix}\frac{E_{11}(z)}{1-\upsilon_{12}(z)\upsilon_{21}(z)} & \frac{\upsilon_{12}(z)\,E_{22}(z)}{1-\upsilon_{12}(z)\upsilon_{21}(z)} & 0 & 0 & 0\\ \frac{\upsilon_{12}(z)\,E_{22}(z)}{1-\upsilon_{12}(z)\upsilon_{21}(z)} & \frac{E_{22}(z)}{1-\upsilon_{12}(z)\upsilon_{21}(z)} & 0 & 0 & 0\\ 0 & 0 & G_{23}(z) & 0 & 0\\ 0 & 0 & 0 & G_{13}(z) & 0\\ 0 & 0 & 0 & 0 & G_{12}(z)\end{bmatrix}\begin{Bmatrix}\varepsilon_{xx}\\ \varepsilon_{yy}\\ \gamma_{yz}\\ \gamma_{xz}\\ \gamma_{xy}\end{Bmatrix} \tag{19}$$

2.4 Dynamic equations of motion of FG-CNT microplate embedded in an elastic media

Based on the Hamiltonian principle, the dynamic equations of motion could be derived as follows, Reddy (2007):

$$0=\int_{t_1}^{t_2}(\delta K-\delta U+\delta V)\,dt \tag{19}$$

where δU presents the variation of the deformation energy

$$\delta U=\frac{1}{2}\int_{\Omega}\delta(\sigma_{xx}\varepsilon_{xx}+\sigma_{yy}\varepsilon_{yy}+\tau_{xy}\gamma_{xy}+\tau_{xz}\gamma_{xz}+\tau_{yz}\gamma_{yz})d\Omega \tag{20}$$

Using Eqs. (13)

$$\delta U=\int_{\Omega}\begin{pmatrix}N_{xx}\delta u_{0,x}+N_{yy}\delta v_{0,x}\\ +N_{xy}(\delta u_{0,x}+\delta v_{0,x})\\ +M_{xx}\,\delta\phi_{x,x}\ +M_{yy}\delta\phi_{y,y}\\ +M_{xy}(\,\delta\phi_{x,y}+\,\delta\phi_{y,x})\\ +\,Q_{xx}(\delta w_{0,x}+\delta\phi_x)\\ +Q_{yy}(\delta w_{0,y}+\delta\phi_y)\end{pmatrix}d\Omega \tag{21}$$

The variation of the total kinetic energy is expressed as

$$\delta K=\frac{1}{2}\int_0^a\int_0^b\int_{-h/2}^{h/2}\delta\,\rho(z)[(\dot{u}^2+\dot{v}^2+\dot{w}^2)]\,dzdydx \tag{22}$$

In terms of the displacement field, Eq. (22) could be written as

$$\delta K = \int_0^a \int_0^b \int_{-\frac{h}{2}}^{\frac{h}{2}} \rho(z) \begin{bmatrix} (\dot{u}_0 + z\dot{\phi}_x)(\delta\dot{u}_0 + z\delta\dot{\phi}_x) + \\ (\dot{v}_0 + z\dot{\phi}_y)(\delta\dot{v}_0 + z\delta\dot{\phi}_y)\dot{v}^2 + \dot{w}_0\delta\dot{w}_0) \end{bmatrix} dzdydx$$
$$= \int_0^a \int_0^b I_0(\dot{u}_0\delta\dot{u}_0 + \dot{v}_0\delta\dot{v}_0 + \dot{w}_0\delta\dot{w}_0) + I_1(\dot{\phi}_x\delta\dot{u}_0 + \dot{u}_0\delta\dot{\phi}_x + \dot{v}_0\delta\dot{\phi}_y + \dot{\phi}_y\delta\dot{v}_0) + I_2(\dot{\phi}_x\delta\dot{\phi}_x + \dot{\phi}_y\delta\dot{\phi}_y)dydx \quad (23)$$

The variation of external potential energy due to the potential of moving load and the elastic foundation could be expressed as,

$$\delta V = \int_\Omega \left[\begin{matrix} q(x,y,t)\delta w_0 - k_w\delta w_0 \\ +k_p\left(\frac{\partial^2 w_0}{\partial x^2} + \frac{\partial^2 \delta w_0}{\partial x^2} + \frac{\partial^2 w_0}{\partial y^2} + \frac{\partial^2 \delta w_0}{\partial y^2}\right) \end{matrix} \right] d\Omega. \quad (24)$$

where $q(x,y,t)$ is the transverse load and k_w and k_p are linear and shear foundation stiffnesses.

Using the Hamilton principle (Reddy 2007)

$$\int_{t1}^{t2} (\delta K - \delta U + \delta V)dt = 0. \quad (25)$$

By substituting Eqs. (21), (23) and (24) into Eq. (25) and after the integration, setting each coefficient of δu_0, δv_0, δw_0, $\delta\phi_x$ and $\delta\phi_y$ to zero, the equations of motion are:

$$\delta u_0: \frac{\partial N_{xx}}{\partial x} + \frac{\partial N_{xy}}{\partial y} = I_0\frac{\partial^2 u_0}{\partial t^2} + I_1\frac{\partial^2 \phi_x}{\partial t^2}, \quad (26)$$

$$\delta v_0: \frac{\partial N_{xy}}{\partial x} + \frac{\partial N_{yy}}{\partial y} = I_0\frac{\partial^2 v_0}{\partial t^2} + I_1\frac{\partial^2 \phi_y}{\partial t^2},$$
$$\delta w_0: \frac{\partial Q_{xx}}{\partial x} + \frac{\partial Q_{yy}}{\partial y} + q - k_w w_0 + k_p\left(\frac{\partial^2 w_0}{\partial x^2} + \frac{\partial^2 w_0}{\partial y^2}\right) = I_0\frac{\partial^2 w_0}{\partial t^2}, \quad (26)$$
$$\delta\phi_x: \frac{\partial M_{xx}}{\partial x} + \frac{\partial M_{xy}}{\partial y} - Q_{xx} = I_1\frac{\partial^2 u_0}{\partial t^2} + I_2\frac{\partial^2 \phi_x}{\partial t^2},$$
$$\delta\phi_x: \frac{\partial M_{xy}}{\partial x} + \frac{\partial M_{yy}}{\partial y} - Q_{yy} = I_1\frac{\partial^2 v_0}{\partial t^2} + I_2\frac{\partial^2 \phi_y}{\partial t^2}.$$

With the inertia coefficients:

$$(I_0, I_1, I_2) = \int_{-h/2}^{h/2} \rho(z)(1, z, z^2)dz \quad (27)$$

By substituting (NSGT 18), (11, 13 18) into (26)

$$\left(1 - l_m^2\frac{\partial^2}{\partial x^2}\right)\left(A_{11}\frac{\partial^2 u_0}{\partial x^2} + A_{12}\frac{\partial^2 v_0}{\partial x\partial y} + A_{66}\left(\frac{\partial^2 v_0}{\partial x\partial y} + \frac{\partial^2 u_0}{\partial y^2}\right) + B_{11}\frac{\partial^2 \phi_x}{\partial x^2} + B_{12}\frac{\partial^2 \phi_y}{\partial x\partial y} + B_{66}\left(\frac{\partial^2 \phi_y}{\partial x\partial y} + \frac{\partial^2 \phi_x}{\partial y^2}\right)\right) + \left(1 - (ea)^2\frac{\partial^2}{\partial x^2}\right)\left(-I_0\frac{\partial^2 u_0}{\partial t^2} - I_1\frac{\partial^2 \phi_x}{\partial t^2}\right) = 0. \quad (28a)$$

$$\left(1 - l_m^2\frac{\partial^2}{\partial x^2}\right)\left(A_{12}\frac{\partial^2 u_0}{\partial x\partial y} + A_{22}\frac{\partial^2 v_0}{\partial y^2} + A_{66}\left(\frac{\partial^2 u_0}{\partial x\partial y} + \frac{\partial^2 v_0}{\partial x^2}\right) + B_{22}\frac{\partial^2 \phi_y}{\partial y^2} + B_{12}\frac{\partial^2 \phi_x}{\partial x\partial y} + B_{66}\left(\frac{\partial^2 \phi_x}{\partial x\partial y} + \frac{\partial^2 \phi_y}{\partial x^2}\right)\right) + \left(1 - (ea)^2\frac{\partial^2}{\partial x^2}\right)\left(-I_0\frac{\partial^2 v_0}{\partial t^2} - I_1\frac{\partial^2 \phi_y}{\partial t^2}\right) = 0. \quad (28b)$$

$$\left(1 - l_m^2\frac{\partial^2}{\partial x^2}\right)\left(k_s A_{55}\left(\frac{\partial^2 w_0}{\partial x^2} + \frac{\partial \phi_x}{\partial x}\right) + k_s A_{44}\left(\frac{\partial^2 w_0}{\partial y^2} + \frac{\partial \phi_y}{\partial y}\right)\right) + \left(1 - (ea)^2\frac{\partial^2}{\partial x^2}\right)\left(q - k_w w_0 + k_p\left(\frac{\partial^2 w_0}{\partial x^2} + \frac{\partial^2 w_0}{\partial y^2}\right) - I_0\frac{\partial^2 w_0}{\partial t^2}\right) = 0. \quad (28c)$$

$$\left(1 - l_m^2\frac{\partial^2}{\partial x^2}\right)\left(B_{11}\frac{\partial^2 u_0}{\partial x^2} + B_{12}\frac{\partial^2 v_0}{\partial x\partial y} + D_{11}\frac{\partial^2 \phi_x}{\partial x^2} + D_{12}\frac{\partial^2 \phi_y}{\partial x\partial y} + B_{66}\left(\frac{\partial^2 v_0}{\partial x\partial y} + \frac{\partial^2 u_0}{\partial y^2}\right) + D_{66}\left(\frac{\partial^2 \phi_y}{\partial x\partial y} + \frac{\partial^2 \phi_x}{\partial y^2}\right) - k_s A_{55}\left(\frac{\partial w_0}{\partial x} + \phi_x\right)\right) + \left(1 - (ea)^2\frac{\partial^2}{\partial x^2}\right)\left(-I_1\frac{\partial^2 u_0}{\partial t^2} - I_2\frac{\partial^2 \phi_x}{\partial t^2}\right) = 0 \quad (28d)$$

$$\left(1 - l_m^2\frac{\partial^2}{\partial x^2}\right)\left(B_{22}\frac{\partial^2 v_0}{\partial y^2} + B_{12}\frac{\partial^2 u_0}{\partial x\partial y} + D_{22}\frac{\partial^2 \phi_y}{\partial y^2} + D_{12}\frac{\partial^2 \phi_x}{\partial x\partial y} + B_{66}\left(\frac{\partial^2 u_0}{\partial x\partial y} + \frac{\partial^2 v_0}{\partial x^2}\right) + D_{66}\left(\frac{\partial^2 \phi_x}{\partial x\partial y} + \frac{\partial^2 \phi_y}{\partial x^2}\right) - k_s A_{44}\left(\frac{\partial w_0}{\partial y} + \phi_y\right)\right) + \left(1 - (ea)^2\frac{\partial^2}{\partial x^2}\right)\left(-I_1\frac{\partial^2 v_0}{\partial t^2} - I_2\frac{\partial^2 \phi_y}{\partial t^2}\right) = 0. \quad (28e)$$

$$(A_{11}, B_{11}, D_{11}) = \int_{-\frac{h}{2}}^{\frac{h}{2}} (1, z, z^2) Q_{11} dz$$
$$(A_{12}, B_{12}, D_{12}) = \int_{-h/2}^{h/2} (1, z, z^2) Q_{12} dz \quad (29a)$$

$$(A_{22}, B_{22}, D_{22}) = \int_{-\frac{h}{2}}^{\frac{h}{2}} (1, z, z^2) Q_{22} dz$$
$$(A_{66}, B_{66}, D_{66}) = \int_{-h/2}^{h/2} (1, z, z^2) Q_{66} dz \quad (29b)$$

$$A_{44} = \int_{-\frac{h}{2}}^{\frac{h}{2}} Q_{44} dz$$
$$A_{55} = \int_{-h/2}^{h/2} Q_{55} dz \quad (29c)$$

For FGM the transverse shear correction factor k_s is given by (Zhu *et al*. 2012a):

$$k_s = \frac{5}{6 - (\upsilon^m V^m + \upsilon_{12}^{cnt} V_{TCNT})} \quad (30)$$

3. Solution methodology of the dynamic equations of motion

To derive an analytical solution for the derived dynamic equations of motion, consider a nanoplate on an elastic foundation with simply supported boundary conditions, Navier's approach will be used to define the vibration frequencies and displacements. For the classical boundary conditions in (at $x, y = 0$ and $x, y = a, b$)

$$N_{xx} = 0, \quad N_{yy} = 0, \quad N_{xy} = 0, \quad w = 0,$$
$$M_{xx} = 0, \quad M_{yy} = 0, \quad M_{xy} = 0, \quad (31)$$

And for non-classical boundary conditions (at $x, y = 0$ and $x, y = a, b$)

$$\frac{\partial u_0}{\partial x} = 0, \quad \frac{\partial v_0}{\partial x} = 0, \quad Q_{xx}^h = 0,$$
$$Q_{yy}^h = 0, \quad \frac{\partial \phi_x}{\partial x} = 0, \quad \frac{\partial \phi_y}{\partial y} = 0, \quad (32)$$

Assuming the vibration solution is periodic in time, the displacements are in the form:

$$\begin{Bmatrix} w_0(x,t) \\ u_0(x,t) \\ v_0(x,t) \\ \phi_x(x,t) \\ \phi_y(x,t) \end{Bmatrix} = \sum_m \sum_n \begin{Bmatrix} W_{mn} \sin(\alpha x) \sin(\beta y) \\ U_{mn} \cos(\alpha x) \sin(\beta y) \\ V_{mn} \sin(\alpha x) \cos(\beta y) \\ \mathrm{X}_{mn} \cos(\alpha x) \sin(\beta y) \\ \mathrm{Y}_{mn} \sin(\alpha x) \cos(\beta y) \end{Bmatrix} e^{i\omega_{mn} t} \quad (33)$$
$$\alpha = \left(\frac{m\pi}{a}\right), \beta = \left(\frac{n\pi}{b}\right), \; i = \sqrt{-1}$$

where ω_{mn} is the natural vibration frequencies. For any U_{mn}, V_{mn} W_{mn}, X_{mn} and Y_{mn} the series solution (33) satisfies the classical and non-classical boundary conditions in (31) and (33). Substituting Eq. (32) into Eq. (27) the following eigen value equation is derived.

$$(\mathbf{K} - \omega_{mn}^2 \mathbf{M})\mathbf{d} = 0 \quad (34)$$

Table 1 CNT efficiency parameters (Lin and Xiang 2014)

CNT efficiency parameters.	*VTCNT*		
Leather	0.12	0.17	0.28
η_1	0.137	0.142	0.141
η_2	1.022	1.626	1.585
η_3	0.715	1.138	1.109

Here, $\mathbf{d} = \{U_{mn} \;\; V_{mn} \;\; W_{mn} \;\; X_{mn} \;\; Y_{mn}\}^{\boldsymbol{T}}$ are the unknowns to be determined, **K,** and **M** are stiffness and mass matrices, respectively. And the coefficients of them are described as follows:

$$\mathbf{K}_{11} = (A11\alpha^2 + A66\beta^2)c_2,$$
$$\mathbf{K}_{12} = (A12 + A66)\beta\alpha c_2,$$
$$\mathbf{K}_{13} = \mathbf{0}, \; \mathbf{K}_{14} = (B11\alpha^2 + B66\beta^2)c_2,$$
$$\mathbf{K}_{15} = (B12 + B66)\beta\alpha,$$
$$\mathbf{K}_{21} = \mathbf{K}_{12}, \; \mathbf{K}_{22} = (A66\alpha^2 + A22\beta^2)c_2,$$
$$\mathbf{K}_{23} = \mathbf{0}, \mathbf{K}_{24} = \mathbf{K}_{15},$$
$$\mathbf{K}_{25} = (B66\alpha^2 + B22\beta^2)c_2,$$
$$\mathbf{K}_{31} = \mathbf{K}_{32} = 0,$$
$$\mathbf{K}_{33} = (k_s A_{55}\alpha^2 + k_s A_{44}\beta^2)c_2 + \left(k_w + k_p(\alpha^2 + \beta^2)\right)c_1,$$
$$\mathbf{K}_{34} = -k_s A_{55}\alpha c_2, \mathbf{K}_{35} = k_s A_{44}\beta c_2,$$
$$\mathbf{K}_{41} = \mathbf{K}_{14}, \; \mathbf{K}_{42} = \mathbf{K}_{15}, \; \mathbf{K}_{43} = k_s A_{55}\alpha c_2,$$
$$\mathbf{K}_{44} = (D11\alpha^2 + D66\beta^2 + k_s A_{55})c_2,$$
$$\mathbf{K}_{45} = (D12 + D66)\beta\alpha c_2,$$
$$\mathbf{K}_{51} = \mathbf{K}_{42}, \; \mathbf{K}_{52} = \mathbf{K}_{25}, \mathbf{K}_{53} = \mathbf{K}_{35},$$
$$\mathbf{K}_{54} = (D22 + D66)\beta\alpha c_2,$$
$$\mathbf{K}_{55} = (D66\alpha^2 + D22\beta^2 + k_s A_{44})c_2, \quad (35)$$
$$\mathbf{M}_{11} = I_0 c_1, \mathbf{M}_{12} = 0, \mathbf{M}_{13} = 0, \mathbf{M}_{14} = I_1 c_1, \; \mathbf{M}_{15} = 0,$$
$$\mathbf{M}_{21} = 0, \mathbf{M}_{22} = I_0 c_1, \mathbf{M}_{23} = 0, \mathbf{M}_{24} = 0, \mathbf{M}_{25} = I_1 c_1$$
$$\mathbf{M}_{31} = \mathbf{0}, \mathbf{M}_{32} = \mathbf{0}, \mathbf{M}_{33} = I_0 c_1, \mathbf{M}_{34} = 0, \mathbf{M}_{35} = 0,$$
$$\mathbf{M}_{41} = \mathbf{M}_{25}, \mathbf{M}_{42} = \mathbf{M}_{43} = 0,$$
$$\mathbf{M}_{44} = I_2 c_1, \mathbf{M}_{45} = 0$$
$$\mathbf{M}_{51} = 0, \mathbf{M}_{52} = I_1 c_1,$$
$$\mathbf{M}_{53} = 0, \mathbf{M}_{54} = 0, \mathbf{M}_{55} = I_2 c_1$$
$$c_1 = 1 + (ea)^2\beta^2, \; c_2 = 1 + l_m^2\beta^2$$

For the forced vibration response of the FG nano plate, substituting Eq. (31) into (26) one can derive the following equation:

$$\mathbf{M}\ddot{\mathbf{d}} + \mathbf{K}\,\mathbf{d} = \mathbf{F}. \quad (36)$$

where **F** is the external force vector and it can be defined according to the type of the transverse load $q(x)$ as given below (Reddy 2007):

$$\mathbf{F} = \begin{Bmatrix} 0 \\ 0 \\ Q_{mn}c_1 \\ 0 \\ 0 \end{Bmatrix} \tag{37}$$

The external load can be expanded in Fourier series and the term Q_{mn} is defined as follows:

$$q(x) = \sum_m \sum_n Q_{mn} \sin(\alpha x) \sin(\beta y) \tag{38a}$$

$$Q_{mn} = \frac{4}{ab}\int_0^a \int_0^b q(x) \sin(\alpha x) \sin(\beta y)\, dxdy \tag{38b}$$

For point load at (x_p, y_p), the external load is defined as $q(x,y,t) = F\delta(x-x_p, y-y_p)$ and Q_{mn} is derived as:

$$\begin{aligned} &Q_{mn} = \frac{4F}{ab}\int_0^a \int_0^b \sin\left(\frac{m\pi}{a}(x_p = vt)\right) \sin\left(\frac{n\pi}{b}y_p\right) dxdy, \\ &m,n = 1,3,5,\ldots \\ &x_p, y_p = a, \frac{b}{2}; \xrightarrow{yields} Q_{mn} = \frac{4F}{ab}\sin\frac{m\pi}{2}\sin\frac{n\pi}{2}, \\ &m,n = 1,3,5,\ldots \end{aligned} \tag{39}$$

For uniform load (Tran *et al*. 2020):

$$\begin{aligned} q(x) &= q_0, \\ Q_{mn} &= \frac{16q_0}{mn\pi^2}, m,n = 1,3,5,\ldots \end{aligned} \tag{40}$$

Dimensionless foundation parameters are defined by (Duc *et al*. 2017)

$$K_1 = \frac{k_w a^4}{E_m h^3}, \qquad K_2 = \frac{k_p a^2}{E_m h^3} \tag{41}$$

4. Verification of the solution procedure

4.1 Verification of CNT nanoplate

To check the accuracy of the derived analytical solution, consider a simply supported composite square plate with the following material and geometrical characteristics: $E^m = 2.5\ GPa$, $\upsilon^m = 0.3$, $E_{11}^{cnt} = 5646.6\ GPa$, $E_{22}^{cnt} = 7080\ GPa$, $G_{12}^{cnt} = 1944.5\ GPa$, $\upsilon_{12}^{cnt} = 0.175$, $\rho^m = 1190\ kg/m^3$, $\rho^{cnt} = 2100\ kg/m^3$, $h = 0.1\ m$, with the efficiency parameters of CNT in Table 1. (Lin and Xiang 2014, Shen and Xiang 2012).

Comparison of the obtained results and the corresponding Numerical ANSYS results and those obtained by obtained by (Thang 2021, Zhu *et al*. 2012a) for different CNT nanoplate configurations are shown in Tables 2 and 3. It is seen that both results are in a good agreement.

4.2 Verification of an isotropic plate on an elastic foundation

To check and verify the efficiency of the obtained solution to effectively investigate the dynamic behavior of an isotropic plate rested on an elastic foundation, consider a simply supported square plate rested on two parameters elastic foundation. The plate is made of (Aluminum, Al) with the following material properties: E_m = 70 GPa; υ = 0.3; ρ_m = 2702 kg/m^3. The developed procedure is applied to detect the free vibration behavior of the plate. The non-dimensional frequency parameter λ, is defined as $\lambda = \omega a^2\sqrt{\rho h/D}$, $(D = Eh^3/12(1-\nu))$. Comparisons of the obtained fundamental frequency λ *o*f the plate at different values of the elastic foundation parameters for different values of thickness to length ratio, (*h*/*a*) are reported in Tables 4 and 5. It may be noticed that the obtained results are conformal with the corresponding results reported in the literature, (Atmane *et al*. 2010, Benferhat *et al*. 2016, Matsunaga 2008, Thai and Choi 2012), verifying the accuracy of the proposed procedure.

5. Numerical results and discussions

To demonstrate the capability of the verified solution procedure to study and analyzed the dynamic behavior of FGCNT nanoplate embedded in an elastic media under moving load, consider A square SSSS FG nanoplate with material characteristics presented in section 4.1. The plate has the following geometrical characteristics: the plate dimensions a=b=100×10^{-9} m and the plate thickness h=0.1a otherwise stated. Both free and forced vibration behaviors are investigated and analyzed.

5.1 Free vibration behavior

To analyze the free vibration behavior, the following expression for the non-dimensional frequency $\lambda_{mn} = \omega_{mn}a^2\sqrt{\rho_m/(E_m h^2)}$ with ρ_m and E_m are the mass density and the elastic modulus of the matrix. Variations of the dimensionless frequencies λ_{11} with the nonlocal parameters, $e_0 a$ at different values of the volume fraction, V_{TCNT} and material length scale parameter, l_m for different elastic foundation parameters and different CNT nanoplate configurations are illustrated in Tables 6-9. It is seen that increasing the reinforcement CNT volume fraction increases the dimensionless frequency parameters for all reinforcement configurations due to increasing the overall system stiffness. Additionally, introduction of the non-classical nonlocal effect at a constant value of the material length scale parameter decreases the dimensionless frequency parameters due to increasing the material compliance. On the other hand, incorporating the non-classical size effect increases the system rigidity and results in larger values of the dimensionless frequency parameters for all CNT configurations at all reinforcement volume fractions.

The elastic foundation stiffness parameters significantly affects the dimensionless frequency parameters for both classical and non-classical free vibration behaviors. Increasing the elastic foundation parameters increases the overall systems stiffness and results in larger values of the dimensionless frequency parameters compared with the corresponding values with zero elastic foundation parameters.

Table 2 Comparison of non-dimensional frequencies $\lambda = \omega_i a^2\sqrt{\rho_m/(E_m h^2)}$ for the effects of widthto-thickness ratio and CNT volume fraction, SSSS square UD and FGΛ plates

$VTCNT$	b/h	Modes (m,n)	UD				FGΛ			
			Present	ANSYS	Zhu *et al*. 2012a	Thang 2021	Present	ANSYS	Zhu *et al*. 2012a	Thang 2021
0.17	10	(1,1)	14.9412	14.9501	16.815	15.3333	13.7671	13.7675	15.461	14.1528
		(1,2)	22.0125	22.0121	22.063	-	21.4908	21.4901	21.307	-
		(1,3)	24.3326	24.3325	24.337	-	24.4857	24.4853	24.511	-
		(1,4)	24.3348	24.3345	24.337	-	24.4851	24.4854	24.511	-
		(2,1)	34.1414	34.1415	34.448	-	34.4942	34.4942	34.273	-
		(2,2)	40.5359	40.5356	40.630	-	39.2374	39.2371	39.263	-
0.17	20	(1,1)	21.4227	21.4223	21.456	-	18.6285	18.6283	18.638	-
		(1,2)	26.6158	26.6155	26.706	-	24.6996	24.6995	24.734	-
		(1,3)	39.9779	39.9774	40.401	-	39.0483	39.0484	39.471	-
		(1,4)	48.6695	48.6694	48.674	-	48.9724	48.9723	49.023	-
		(2,1)	48.6695	48.6694	48.674	-	48.9723	48.9721	49.023	-
		(2,2)	61.3728	61.3725	62.723	-	58.8556	58.8552	59.191	-

Table 3 Comparison of non-dimensional frequencies $\lambda = \omega_i a^2\sqrt{\rho_m/(E_m h^2)}$ for the effects of width-to-thickness ratio and CNT volume fraction, SSSS square FGO and FGX plates

$VTCNT$	b/h	Modes (m,n)	FGO				FGX			
			Present	ANSYS	Zhu *et al*. 2012a	Thang 2021	Present	ANSYS	Zhu *et al*. 2012a	Thang 2021
0.17	10	(1,1)	12.7985	12.7988	14.282	13.0976	16.2192	16.2193	18.278	16.6524
		(1,2)	20.2693	20.2694	20.091	-	23.7606	23.7605	23.541	-
		(1,3)	24.4862	24.4864	24.512	-	24.4866	24.4845	24.512	-
		(1,4)	24.4865	24.4867	24.512	-	24.4863	24.4867	24.512	-
		(2,1)	32.9834	32.9831	32.766	-	36.5119	36.5126	36.245	-
		(2,2)	37.7551	37.7553	37.763	-	42.1311	42.1319	42.150	-
0.17	20	(1,1)	16.6402	16.6403	16.628	-	24.7352	24.7345	24.764	-
		(1,2)	22.7103	22.7105	22.739	-	29.8093	29.8029	29.819	-
		(1,3)	36.7195	36.7194	37.139	-	43.2574	43.2565	43.612	-
		(1,4)	48.9726	48.9723	49.024	-	48.9728	48.9735	49.024	-
		(2,1)	48.9724	48.9724	49.024	-	48.9724	48.9735	49.024	-
		(2,2)	54.0993	54.0998	54.367	-	65.0743	65.0737	66.616	-

Table 4 Comparisons of the fundamental frequency parameters λ_{mn} for simply supported isotropic square plate embedded in an elastic media, m, n = 1, for different values of the thickness to length ratio at different foundation parameters

Thickness to length ratio h/a	K_1, K_2	Theory		
		(Atmane *et al*. 2010)	(Benferhat *et al*. 2016)	Present
0.001	0, 0	19.7392	19.7320	19.7362
	10^2, 10	26.2112	26.2048	26.2106
	10^3, 10^2	57.9962	57.9894	57.9891
0.1	0, 0	19.0658	19.0660	19.0662
	10^2, 10	25.6236	25.5989	25.6012
	10^3, 10^2	57.3923	57.2775	57.2915
0.2	0, 0	17.4531	17.4553	17.4534
	10^2, 10	24.2728	24.1068	24.2364
	10^3, 10^2	56.0311	56.0260	56.0287

Table 5 Comparisons of the non-dimensional natural frequencies $\lambda_{m,n}$ for a simply supported isotropic square plate resting on an elastic foundation for different values of elastic foundation parameters at (h/b =0.2)

K_1	K_2	$\lambda_{1,1}$			$\lambda_{1,2}$			$\lambda_{1,3}$		
		Matsunaga 2008	Thai and Choi 2012	Present	Matsunaga 2008	Thai and Choi 2012	Present	Matsunaga 2008	Thai and Choi 2012	Present
0		17.5260	17.4523	17.4556	38.4827	38.1883	38.2021	65.9961	65.3135	65.3734
10		17.7847	17.7248	17.7346	38.5929	38.3098	38.3045	66.0569	65.3841	65.6735
10^2	0	19.9528	20.0076	19.9567	39.5669	39.3895	39.3812	66. 5995	66.0138	66.0575
10^3		34.3395	35.5039	35.4576	47.8667	48.8772	48.3524	71.5577	72.0036	71.5789
10^4		45.5260	45.5255	45.5256	71.9829	71.9829	71.9865	97.4964	101.7990	101.7991
0		22.0429	22.2145	22.0732	43.4816	43.7943	43.6245	71.4914	71.9198	71.4846
10		22.2453	22.4286	22.3454	43.5747	43.9009	43.8534	71.5423	71.9839	71.8945
10^2	10	23.9830	24.2723	24.1442	44.3994	44.8445	44.6587	71.9964	72.5554	72.0346
10^3		36.6276	38.0650	37.6367	51.6029	53.3580	52.7523	76.1848	78.0290	77.0765
10^4		45.5260	45.5255	45.5238	71.9829	71.9829	71.9832	99.0187	101.7990	101.7943

Table 6 Variations of the dimensionless frequencies λ_{mn} and m = 1, n = 1 of SSSS square UD-CNT nanoplate with the nonlocality parameter, e_0a for different values of the volume fraction, V_{TCNT} and material size parameter, l_m (nm) for b, a/h = 10 at different values of elastic foundation parameters

	V_{TCNT} = 0.12			V_{TCNT} = 0.17			V_{TCNT} = 0.28		
e_0a	l_m = 0	l_m = 1	l_m = 2	l_m = 0	l_m = 1	l_m = 2	l_m = 0	l_m = 1	l_m = 2
					$K_1 = K_2 = 0$				
0	12.038725	13.151692	16.159082	14.941245	16.322550	20.055025	16.337574	17.847961	21.929247
0.5	11.892899	12.992385	15.963345	14.760261	16.124832	19.812096	16.139675	17.631763	21.663614
1	11.019946	12.038728	14.791618	13.676843	14.941248	18.357862	14.955005	16.337574	20.073477
1.5	10.048860	10.977864	13.488170	12.471627	13.624619	16.740156	13.637161	14.897894	18.304588
2	8.9690037	9.7981768	12.038727	11.131421	12.160510	14.941252	12.171704	13.296961	16.337570
					$K_1 = 10^2$, $K_2 = 10$				
0	20.368944	21.045975	23.045345	22.000311	22.960838	25.748432	22.577835	23.693741	26.902384
0.5	20.283087	20.946779	22.908510	21.877796	22.820702	25.559671	22.435043	23.531309	26.686296
1	19.783789	20.368944	22.107954	21.161911	22.000309	24.449699	21.598444	22.577833	25.412401
1.5	19.259649	19.760376	21.257885	20.403662	21.128195	23.259579	20.707733	21.558937	24.039598
2	18.718712	19.130009	20.368942	19.613062	20.214968	22.000315	19.773344	20.485283	22.577829

Table 7 Variations of the dimensionless frequencies λ_{mn} and m = 1, n = 1 of SSSS square FGV -CNT nanoplate with the nonlocality parameter, e_0a for different values of the volume fraction, V_{TCNT} and material size parameter, l_m (nm) for b, a/h = 10 at different values of elastic foundation parameters

	V_{TCNT} = 0.12			V_{TCNT} = 0.17			V_{TCNT} = 0.28		
e_0a	l_m = 0	l_m = 1	l_m = 2	l_m = 0	l_m = 1	l_m = 2	l_m = 0	l_m = 1	l_m = 2
					$K_1 = K_2 = 0$				
0	10.686799	11.674780	14.344450	13.855944	15.136909	18.598253	14.850828	16.223764	19.933662
0.5	10.557340	11.533368	14.170682	13.688095	14.953542	18.372967	14.670941	16.027246	19.692198
1	9.7824154	10.686796	13.130547	12.683378	13.855944	17.024380	13.594081	14.850824	18.246758
1.5	8.9203892	9.7450714	11.973473	11.565701	12.634942	15.524173	12.396149	13.542160	16.638857
2	7.9617968	8.6978645	10.686796	10.322859	11.277193	13.855949	11.064066	12.086924	14.850842
					$K_1 = 10^2$, $K_2 = 10$				
0	17.442204	19.054619	23.411634	22.385475	24.454899	30.046850	23.440327	25.607199	31.462652
0.5	17.230925	18.823805	23.128040	22.114346	24.158705	29.682861	23.156315	25.297098	31.081553
1	15.966255	17.442213	21.430481	20.491184	22.385466	27.504196	21.456621	23.440302	28.800135
1.5	14.559433	15.905316	19.542103	18.685577	20.412930	25.080566	19.566048	21.374743	26.262354
2	12.995030	14.196251	17.442207	16.677706	18.219446	22.385509	17.463501	19.077919	23.440283

Table 8 Variations of the dimensionless frequencies λ_{mn} and m = 1, n = 1 of SSSS square FGX -CNT nanoplate with the nonlocality parameter, e_0a for different values of the volume fraction, V_{TCNT} and material size parameter, l_m (nm) for b, a/h = 10 at different values of elastic foundation parameters

	V_{TCNT} = 0.12			V_{TCNT} = 0.17			V_{TCNT} = 0.28		
e_0a	l_m = 0	l_m = 1	l_m = 2	l_m = 0	l_m = 1	l_m = 2	l_m = 0	l_m = 1	l_m = 2
					$K_1 = K_2 = 0$				
0	12.937205	14.133233	17.365076	16.219255	17.718702	21.770428	19.270245	21.051762	25.865713
0.5	12.780496	13.962032	17.154734	16.022785	17.504074	21.506725	19.036686	20.796711	25.552195
1	11.842390	12.937205	15.895555	14.846698	16.219252	19.928106	17.639385	19.270136	23.676624
1.5	10.798834	11.797169	14.494830	13.538399	14.790000	18.172028	16.084980	17.572102	21.590282
2	9.6383848	10.529440	12.937208	12.083556	13.200660	16.219254	14.356524	15.683754	19.270256
					$K_1 = 10^2$, $K_2 = 10$				
0	20.914026	21.674335	23.907747	22.888529	23.974470	27.106785	38.540474	42.103569	51.731392
0.5	20.817440	21.563080	23.755398	22.749725	23.816273	26.895447	38.073574	41.593361	51.104313
1	20.254961	20.914028	22.862648	21.937244	22.888531	25.650618	35.278809	38.540329	47.353325
1.5	19.662937	20.228554	21.911856	21.073765	21.898912	24.311432	32.170341	35.144417	43.180584
2	19.050125	19.516247	20.914024	20.169867	20.858381	22.888529	28.713062	31.367441	38.540405

Table 9 Variations of the dimensionless frequencies λ_{mn} and m = 1, n = 1 of SSSS square FGO -CNT nanoplate with the nonlocality parameter, e_0a for different values of the volume fraction, V_{TCNT} and material size parameter, l_m (nm) for b, a/h = 10 at different values of elastic foundation parameters

	V_{TCNT} = 0.12			V_{TCNT} = 0.17			V_{TCNT} = 0.28		
e_0a	l_m = 0	l_m = 1	l_m = 2	l_m = 0	l_m = 1	l_m = 2	l_m = 0	l_m = 1	l_m = 2
					$K_1 = K_2 = 0$				
0	10.419436	11.382705	13.985586	12.798543	13.981762	17.178961	14.302255	15.624480	19.197325
0.5	10.293223	11.244823	13.816178	12.643513	13.812395	16.970867	14.129004	15.435224	18.964787
1	9.5376892	10.419437	12.802051	11.715461	12.798549	15.725188	13.091923	14.302261	17.572754
1.5	8.6972218	9.5012712	11.673926	10.683086	11.670734	14.339475	11.938253	13.041936	16.024229
2	7.7626128	8.4802608	10.419443	9.5350752	10.416594	12.798547	10.655363	11.640440	14.302255
					$K_1 = 10^2$, $K_2 = 10$				
0	19.449648	19.982325	21.571505	20.599897	21.355196	23.572762	21.148546	22.064272	24.723417
0.5	19.382315	19.904095	21.462049	20.503933	21.244692	23.421532	21.031765	21.930653	24.543295
1	18.991781	19.449652	20.823627	19.944996	20.599901	22.535273	20.349529	21.148546	23.484266
1.5	18.583782	18.973513	20.149660	19.356562	19.918751	21.591105	19.627144	20.317398	22.349138
2	18.164967	18.483198	19.449650	18.747309	19.210743	20.599899	18.874231	19.447420	21.148544

5.2 Forced vibration behavior of FGCNT nanoplate under moving load

The Newmark numerical integration methodology is exploited to obtain the forced vibration time response of FGCNT nanoplate embedded in an elastic foundation and subjected to a moving point load of intensity 1 nN. The time increment is taken as $\Delta t=T_{final}/500$, $T_{final}=L/v$. The dimensionless speed parameter, β is applied as $\beta=v/v_{crital}$, when β=1 means the load velocity is equal to first critical speed of the plate The normalized maximum midspan transverse deflection is defined by using the static midpoint deflection of the plate without any CNT addition. $W_{rel} = \frac{W(L/2,t)}{W_{static}(L/2)|_{NoCNT}}$.

Variations of the maximum normalized midspan deflections, W_{rel} with the dimensionless moving load speed parameter, β for different nanoplate CNT reinforcement configurations for different volume fractions, V_{TCNT} are illustrated in Fig. 3. It is seen that the reinforcement configuration and its volume fraction and significantly affect the maximum normalized midspan transverse deflection profiles over the dimensionless moving load speed parameter, β. Increasing the reinforcement volume fraction increases the system stiffness which decreases the material flexibility this produces smaller values of the maximum normalized midspan transverse deflection for all reinforcement configurations. Comparing between the different reinforcement configurations, the FGO-CNT produces more flexible systems and resulting in

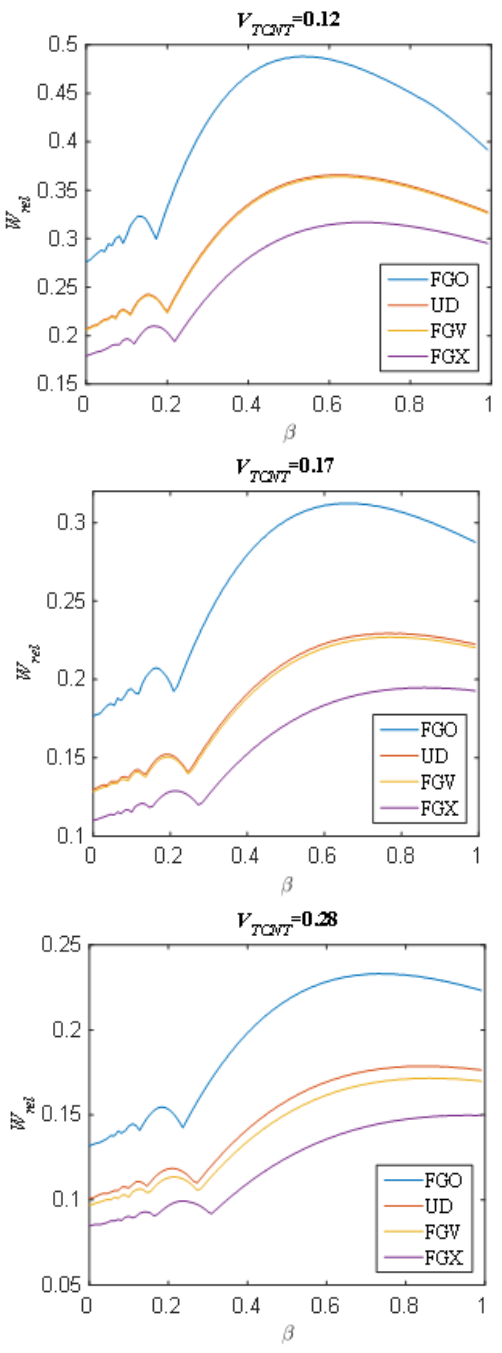

Fig. 3 Variations of the maximum normalized midspan deflections, W_{rel} with the dimensionless moving load speed parameter, β for different nanoplate CNT reinforcement configurations for different volume fractions, V_{TCNT} at FG power-law exponent k=1 in FGV-CNT, FGX-CNT and FGO-CNT for $K_1 = K_2 = 0$

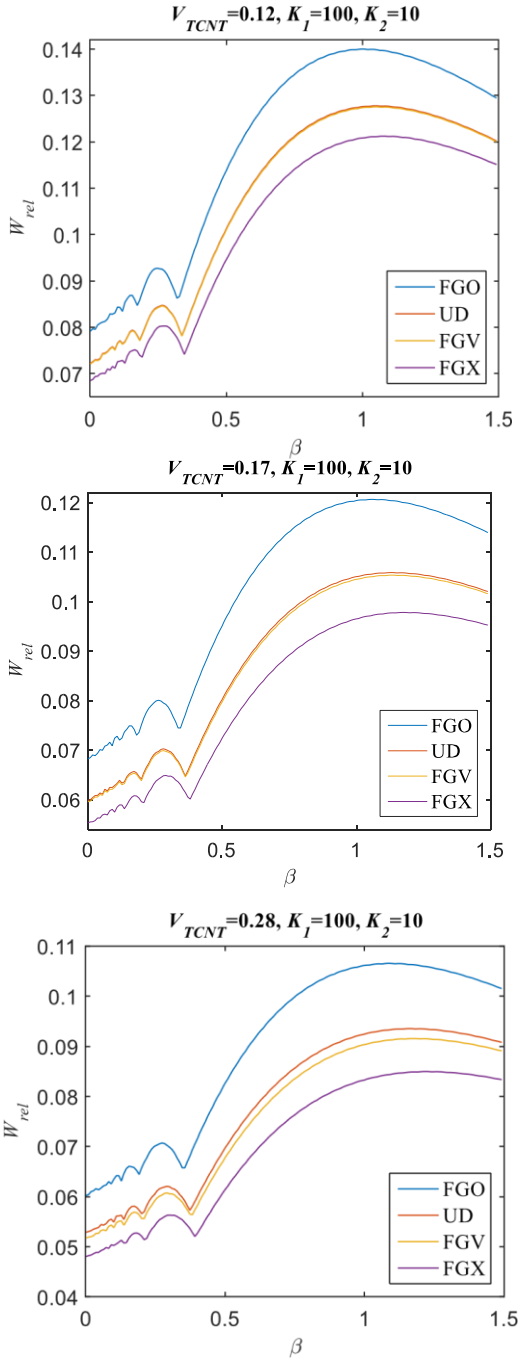

Fig. 4 Variations of the maximum normalized midspan deflections, W_{rel} with the dimensionless moving load speed parameter, β for different nanoplate CNT reinforcement configurations for different volume fractions, V_{TCNT} at FG power-law exponent k=1 in FGV- CNT, FGX-CNT and FGO-CNT at $K_1 = 10^2$, $K_2 = 10$

larger values of the maximum normalized midspan transverse deflection compared with those produced by UD_CNT, FGV-CNT, and FGX-CNT configurations for all reinforcement volume fractions.

Incorporating the elastic foundation stiffness significantly affects the forced vibration response under moving load. The dependency of the maximum normalized midspan deflections, W_{rel} on the dimensionless moving load speed parameter, β for different nanoplate CNT reinforcement configurations for different volume fractions, V_{TCNT} and elastic foundation stiffness parameters, K_1 and K_2 are depicted in Fig. 4.

It is observed that increasing the elastic foundation stiffness parameters increases the overall system rigidity which results in lower values of the maximum normalized midspan transverse deflection compared with the

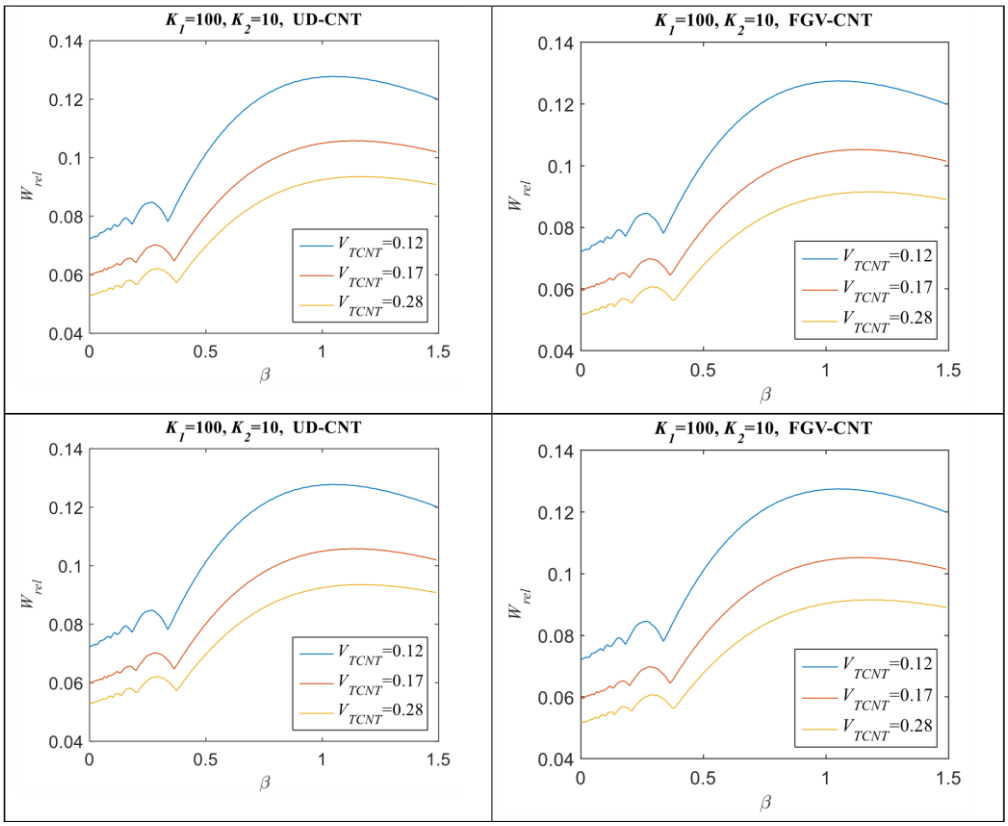

Fig. 5 Variations of the maximum normalized midspan deflections, W_{rel} with the dimensionless moving load speed parameter, β for different nanoplate CNT reinforcement configurations for different volume fractions, V_{TCNT} at FG power-law exponent k=1 in FGV-CNT, FGX-CNT and FGO-CNT

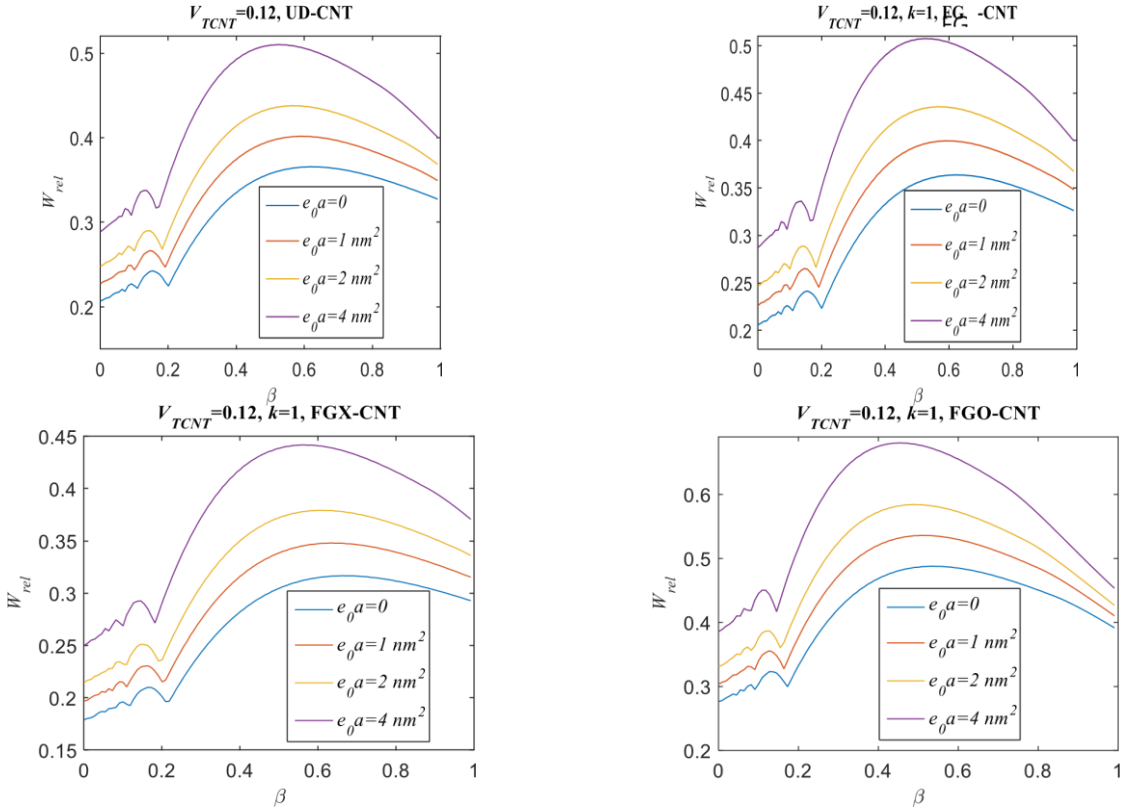

Fig. 6 Variations of the maximum normalized midspan deflections, W_{rel} with the dimensionless moving load speed parameter, β for different nanoplate CNT reinforcement configurations for different values of the nonlocal parameters, e_0a at FG power-law exponent k=1 , V_{TCNT} = 0.12 and l_m = 0 in FGV-CNT, FGX-CNT and FGO-CNT. $K_1 = K_2 = 0$

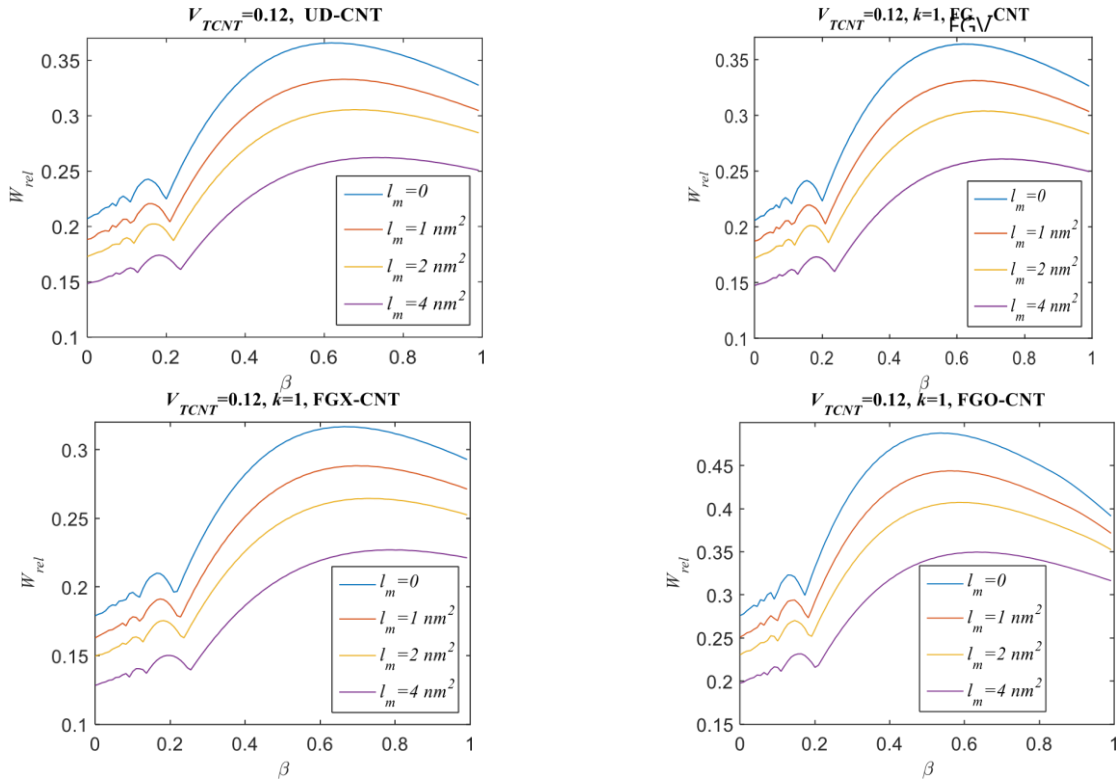

Fig. 7 Variations of the maximum normalized midspan deflections, W_{rel} with the dimensionless moving load speed parameter, β for different nanoplate CNT reinforcement configurations for different values of the material length scale parameters, l_m at FG power-law exponent k=1, V_{TCNT} = 0.12 and e_0a =0 in FGV-CNT, FGX-CNT and FGO-CNT. K_1 = K_2 = 0

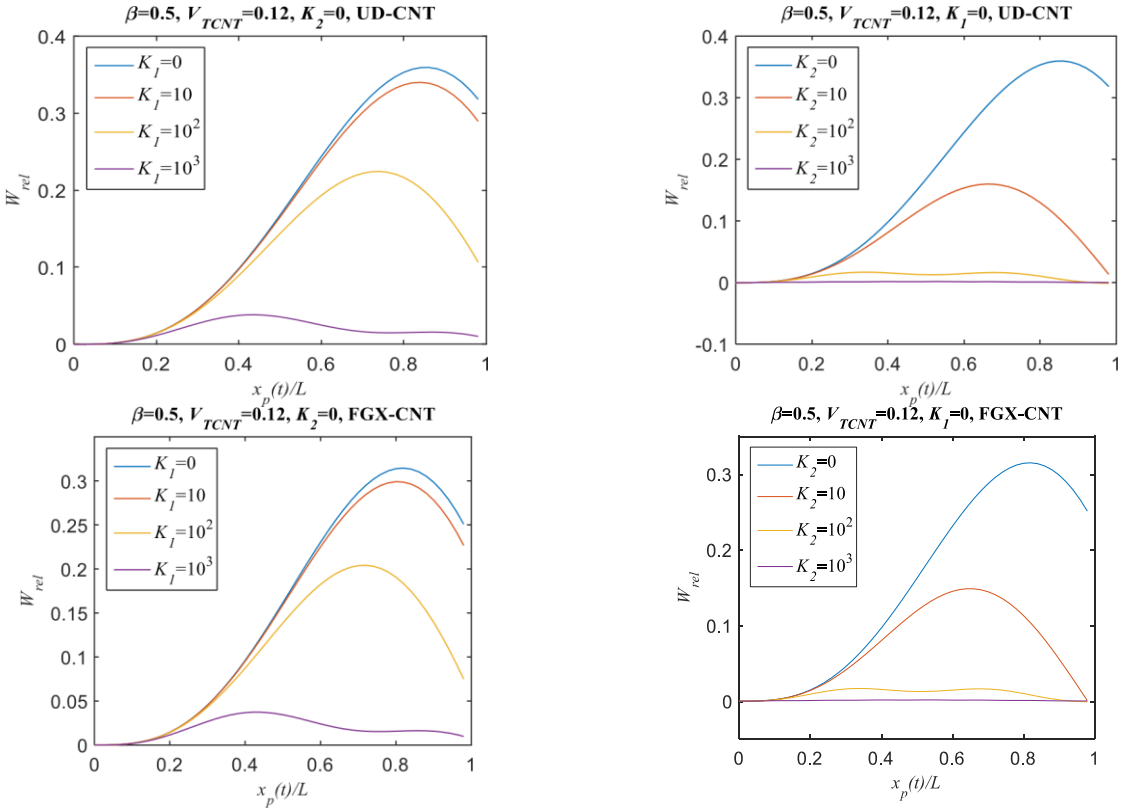

Fig. 8 The maximum normalized midspan deflections, W_{rel} profiles over the normalized longitudinal spatial coordinate, $x_p(t)/L$ for different nanoplate CNT reinforcement configurations for different values of the elastic foundation stiffness constants at FG power-law

corresponding cases without elastic foundation for all nanoplate CNT configurations and volume fractions. In contrary to the corresponding cases without elastic foundation, the maximum value of the normalized midspan transverse deflection with elastic foundation is reached at dimensionless speed parameter $\beta>1$.

Comparisons between the maximum normalized midspan transverse deflection profiles over the dimensionless speed parameters, β for different reinforcement CNT configurations at different values of volume fractions are depicted in Fig. 5. It is noticed that increasing either the elastic foundation stiffness or the reinforcement volume fraction produces smaller values of the maximum normalized midspan deflections due to increasing the material rigidity for all CNT configurations.

Incorporating the nonlocality effect in the absence of the microstructure size effect results in increasing the system flexibility and resulting in larger values of the maximum normalized midspan transverse deflection for all CNT configurations, as shown in Fig.6. Moreover, increasing the nonlocality parameter results in reaching the maximum value of the normalized midspan transverse deflection at smaller value of the dimensionless speed parameter, β for all CNT nanoplate configurations.

On contrary to the obtained response due to incorporating the nonlocal effect, increasing the material length scale parameter at zero nonlocality parameter decreases the system flexibility and produces smaller values of the maximum normalized midspan transverse deflection for all CNT configurations, as shown in Fig. 7. Additionally, increases the material length scale parameter increases the dimensionless speed parameter, β required to reach the maximum value of the normalized midspan transvers deflection for all CNT nanoplate configurations.

Comparisons of the effect of increasing the elastic foundation stiffness parameters, K_1 and K_2 on the maximum normalized midspan transverse deflection profiles throughout the normalized longitudinal spatial coordinate for different CNT nanoplate configurations are shown in Fig. 8. Generally, increasing the elastic stiffness foundation parameters increases the overall system rigidity which decreases the maximum normalized transverse deflection for all CNT configurations. Moreover, increasing the elastic foundation stiffness parameter, K_2 has more significant effect on the maximum normalized midspan deflection throughout the normalized longitudinal spatial coordinates, larger drop in the maximum normalized midspan deflection is observed compared with the corresponding cases of K_1. Additionally, the location at which the maximum normalized midspan deflection is also affected by increasing the elastic foundation stiffness parameters, this location moves towards the origin as the elastic foundation stiffness parameter increases.

6. Conclusions

A comprehensive numerical investigation of the non-classical size dependent dynamic behavior of composite functionally graded CNT nanoplate rested on two parameters elastic foundation and subjected to moving load based on the nonlocal strain gradient elasticity theory (NSGET) is presented. The accuracy of the developed solution procedure is verified and compared. Numerical results are obtained and discussed. Based on the obtained numerical results the following concluding remarks are revealed:

- The dynamic behaviour of FGCNT nanoplate embedded in elastic foundation is significantly affected by the two parameters of the elastic foundation. Both free and forced vibration behaviors could be controlled by controlling the elastic foundation stiffness parameters.
- Increasing the elastic foundation parameters increases the system rigidity and produces larger values of the dimensionless frequency parameters for all CNT configurations at all values of volume fractions.
- The maximum normalized midspan dynamic deflection is significantly affected by increasing the elastic foundation stiffness parameters. Due to decreasing the system flexibility associated with increasing the elastic foundation stiffness parameters, the maximum normalized transverse dynamic deflection decreases. Also, both the moving load speed that required to reach the maxim transverse dynamic deflection and the normalized spatial coordinate at which the maximum transverse deflection occurs are decreased with increasing the elastic foundation stiffness parameters.
- Depending on the dimensionless speed parameter of the moving load, the stability of the maximum normalized midspan transverse deflection profiles throughout the normalized longitudinal coordinate are significantly affected by increasing the elastic foundation stiffness parameters. Increasing the elastic foundation stiffness parameters decreases the number of oscillations in these profiles. At higher values of these stiffness parameters, the system behaves quasi-statically.
- The reinforcement CNT volume fraction significantly affects the dynamic behaviour of FGCNT nanoplate. Increasing this volume fraction increases the system rigidity thus increases the resonant frequencies and decreases the forced time response under moving load. So, both free and forced vibration behaviors could be controlled by controlling the CNT volume fraction.
- In addition to the reinforcement volume fraction, the FGCNT configuration has a significant effect on the free and forced vibration behaviors. The FGX-CNT results in a more rigid nanoplate this increases the resonant frequencies and decreases the forced vibration time response under moving load. On contrary to the FGX-CNT, FGO-CNT configuration produces a more compliant nanoplate thus smaller values of the resonant frequencies and larger values of the forced vibration time response are detected compared with the corresponding cases obtained by the other CNT configurations.
- Incorporating the non-classical material parameters greatly affects the free and forced vibration behaviour of FGCNT nanoplate. Introduction of the nonlocality effect resulting in softening effect while introducing the material length scale size effect leads to hardening effect. Thus, the dynamic behaviour could be controlled by controlling theses nonclassical parameters.

Acknowledgments

This project was funded by the Deanship of Scientific Research (DSR) at King Abdulaziz University, Jeddah, under grand no. (GPIP: 375-135-2024). The Authors, therefore, acknowledge with thanks DSR for technical and financial support.

References

Abdelrahman, A.A., Esen, I., Daikh, A.A. and Eltaher, M.A. (2021c), "Dynamic analysis of FG nanobeam reinforced by carbon nanotubes and resting on elastic foundation under moving load", *Mech. Based Des. Struct.*, 1-24. https://doi.org/10.1080/15397734.2021.1999263

Abdelrahman, A.A., Esen, I., Özarpa, C. and Eltaher, M.A. (2021b), "Dynamics of perforated nanobeams subject to moving mass using the nonlocal strain gradient theory", *Appl. Math. Modell.*, **96**, 215-235. https://doi.org/10.1016/j.apm.2021.03.008

Abdelrahman, A.A., Esen, I., Ozarpa, C., Shaltout, R., Eltaher, M. A. and Assie, A.E. (2021a), "Dynamics of perforated higher order nanobeams subject to moving load using the nonlocal strain gradient theory", *Smart Struct. Syst.*, **28**(4), 515-533. https://doi.org/10.12989/sss.2021.28.4.515

Abo-Bakr, H.M., Abo-Bakr, R.M., Mohamed, S.A. and Eltaher, M.A. (2020), "Weight optimization of axially functionally graded microbeams under buckling and vibration behaviors", *Mech. Based Des. Struct.*, 1-22. https://doi.org/10.1080/15397734.2020.1838298

Alazwari, M.A., Daikh, A.A., Houari, M.S.A., Tounsi, A. and Eltaher, M.A. (2021), "On static buckling of multilayered carbon nanotubes reinforced composite nanobeams supported on non-linear elastic foundations", *Steel Compos. Struct.*, **40**(3), 389-404. https://doi.org/10.12989/scs.2021.40.3.389

Analooei, H.R., Azhari, M. and Salehipour, H. (2021), "Thermo-electro-mechanical vibration and buckling analysis of quadrilateral and triangular nanoplates with the nonlocal finite strip method", *Mech. Based Des. Struct.*, 1-21. https://doi.org/10.1080/15397734.2021.1875331

Arefi, M. and Soltan Arani, A.H. (2018), "Higher order shear deformation bending results of a magnetoelectrothermoelastic functionally graded nanobeam in thermal, mechanical, electrical, and magnetic environments", *Mech. Based Des. Struct.*, **46**(6), 669-692. https://doi.org/10.1080/15397734.2018.1434002

Assie, A., Akbaş, Ş.D., Bashiri, A.H., Abdelrahman, A.A. and Eltaher, M.A. (2021), "Vibration response of perforated thick beam under moving load", *Eur. Phys. J. Plus*, **136**(3), 1-15. https://doi.org/10.1140/epjp/s13360021-01224-2

Atmane, H.A., Tounsi, A. and Mechab, I. (2010), "Free vibration analysis of functionally graded plates resting on Winkler–Pasternak elastic foundations using a new shear deformation theory", *Int. J. Mech. Mater. Des.*, **6**(2), 113-121. https://doi.org/10.1007/s10999-010-9110-x

Babaei, M., Asemi, K. and Kiarasi, F. (2021), "Dynamic analysis of functionally graded rotating thick truncated cone made of saturated porous materials", *Thin Wall. Struct.*, **164**, 107852. https://doi.org/10.1016/j.tws.2021.107852

Barati, M.R. (2017), "Nonlocal-strain gradient forced vibration analysis of metal foam nanoplates with uniform and graded porosities", *Adv. Nano Res.*, **5**(4), 393. https://doi.org/10.12989/anr.2017.5.4.393

Benferhat, R., Daouadji, T.H. and Mansour, M.S. (2016), "Free vibration analysis of FG plates resting on an elastic foundation and based on the neutral surface concept using higher-order shear deformation theory", *Comptes Rendus Mecanique*, **344**(9), 631-641. https://doi.org/10.1016/j.crme.2016.03.002

Bouafia, H., Chikh, A., Bousahla, A.A., Bourada, F., Heireche, H., Tounsi, A., Benrahou, K.H., Tounsi, A., Al-Zahrani, M.M. and Hussain, M., (2021), "Natural frequencies of FGM nanoplates embedded in an elastic medium", *Adv. Nano Res.*, **11**(3), 239. https://doi.org/10.12989/anr.2021.11.3.239

Bouazza, M. and Zenkour, A.M. (2020), "Vibration of carbon nanotube-reinforced plates via refined n th-higher-order theory", *Arch. Appl. Mech.*, **90**(8), 1755-1769. https://doi.org/10.1007/s00419-020-01694-3

Daikh, A.A., Drai, A., Houari, M.S.A. and Eltaher, M. A. (2020), "Static analysis of multilayer nonlocal strain gradient nanobeam reinforced by carbon nanotubes", *Steel Compos. Struct.*, **36**(6), 643-656. https://doi.org/10.12989/scs.2020.36.6.643

Daikh, A.A., Houari, M.S.A., Karami, B., Eltaher, M.A., Dimitri, R. and Tornabene, F. (2021a), "Buckling Analysis of CNTRC curved sandwich nanobeams in thermal environment", *Appl. Sci.*, **11**(7), 3250. https://doi.org/10.3390/app11073250

Daikh, A. A., Houari, M.S.A., Belarbi, M.O., Chakraverty, S. and Eltaher, M.A. (2021b), "Analysis of axially temperature-dependent functionally graded carbon nanotube reinforced composite plates", *Eng. Comput.*, 1-22. https://doi.org/10.1007/s00366-021-01413-8

Daikh. A.A., Houari, M.S.A. and Eltaher, M.A. (2021c), "A novel nonlocal strain gradient Quasi-3D bending analysis of sigmoid functionally graded sandwich nanoplates", *Compos. Struct.*, **262**, 113347. https://doi.org/10.1016/j.compstruct.2020.113347

Dehshahri, K., Nejad, M.Z., Ziaee, S., Niknejad, A. and Hadi, A. (2020), "Free vibrations analysis of arbitrary threedimensionally FGM nanoplates", *Adv. Nano Res.*, **8**(2), 115-134. https://doi.org/10.12989/anr.2020.8.2.115

Ding, H.X. and She, G.L. (2021), "A higher-order beam model for the snap-buckling analysis of FG pipes conveying fluid", *Struct. Eng. Mech.*, **80**(1), 63-72. http://doi.org/10.12989/sem.2021.80.1.063

Duc, N.D., Lee, J., Nguyen-Thoi, T. and Thang, P.T. (2017), "Static response and free vibration of functionally graded carbon nanotube-reinforced composite rectangular plates resting on Winkler–Pasternak elastic foundations", *Aerosp. Sci. Technol.*, **68**, 391-402. https://doi.org/10.1016/j.ast.2017.05.032

Ebrahimi, F., Dabbagh, A., Tornabene, F. and Civalek, O. (2019), "Hygro-thermal effects on wave dispersion responses of magnetostrictive sandwich nanoplates", *Adv. Nano Res.*, **7**(3), 157. https://doi.org/10.12989/anr.2019.7.3.157

Eglin, M., Eriksson, M.A. and Carpick, R.W. (2006), "Micro-particle manipulation using inertial forces", *Appl. Phys. Lett.*, **88**(9), 091913. https://doi.org/10.1063/1.2172401

Eltaher, M.A., Abdelrahman, A.A. and Esen, I. (2021), "Dynamic analysis of nanoscale Timoshenko CNTs based on doublet mechanics under moving load", *Eur. Phys. J. Plus*, **136**(7), 1-21. https://doi.org/10.1140/epjp/s13360-021-01682-8

Eltaher, M.A., Abdelrahman, A.A., Al-Nabawy, A., Khater, M. and Mansour, A. (2014), "Vibration of nonlinear graduation of nano-Timoshenko beam considering the neutral axis position", *Appl. Math. Comput.*, **235**, 512-529. http://doi.org/10.1016/j.amc.2014.03.028

Esen, I., Abdelrahman, A.A. and Eltaher, M.A. (2020), "Dynamics analysis of timoshenko perforated microbeams under moving loads", *Eng. Comput.*, 1-17. https://doi.org/10.1007/s00366-020-01212-7

Esen, I., Abdelrahman, A.A. and Eltaher, M.A. (2021d), "On vibration of sigmoid/symmetric functionally graded nonlocal strain gradient nanobeams under moving load", *Int. J. Mech. Mater. Des.*, **17**, 721-742. https://doi.org/10.1007/s10999-021-09555-9.

Esen, I., Abdelrhmaan, A.A. and Eltaher, M.A. (2021b), "Free

vibration and buckling stability of FG nanobeams exposed to magnetic and thermal fields", *Eng. Comput.*, 1-20. https://doi.org/10.1007/s00366-021-01389-5

Esen, I., Daikh, A.A. and Eltaher, M.A. (2021c), "Dynamic response of nonlocal strain gradient FG nanobeam reinforced by carbon nanotubes under moving point load", *Eur. Phys. J. Plus*, **136**(4), 1-22. https://doi.org/10.1140/epjp/s13360-021-01419-7

Esen, I., Eltaher, M. A. and Abdelrahman, A.A. (2021e), "Vibration response of symmetric and sigmoid functionally graded beam rested on elastic foundation under moving point mass", *Mech. Based Des. Struct.*, 1-25. https://doi.org/10.1080/15397734.2021.1904255

Esen, I., Özarpa, C. and Eltaher, M.A. (2021a), "Free vibration of a cracked FG microbeam embedded in an elastic matrix and exposed to magnetic field in a thermal environment", *Compos. Struct.*, **261**, 113552. https://doi.org/10.1016/j.compstruct.2021.113552

Esmaeilzadeh, M., Esmaeil Golmakani, M., Kadkhodayan, M., Amoozgar, M. and Bodaghi, M. (2021), "Geometrically nonlinear thermo-mechanical analysis of graphene-reinforced moving polymer nanoplates", *Adv. Nano Res.*, **10**(2), 151-163. https://doi.org/10.12989/anr.2021.10.2.151

Esmaeilzadeh, M., Golmakani, M.E. and Sadeghian, M. (2020), "A nonlocal strain gradient model for nonlinear dynamic behavior of bi-directional functionally graded porous nanoplates on elastic foundations", *Mech. Based Des. Struct.*, 1-20. https://doi.org/10.1080/15397734.2020.1845965

Farahmand, H. (2021), "A variational approach for analytical buckling solution of moderately thick microplate using strain gradient theory incorporating two-variable refined plate theory: A benchmark study", *J. Brazil. Soc. Mech. Sci. Eng.*, **43**(3), 1-11. https://doi.org/10.1007/s40430-020-02766-9

Griebel, M. and Hamaekers, J. (2004), "Molecular dynamics simulations of the elastic moduli of polymer–carbon nanotube composites", *Comput. Meth. Appl. Mech. Eng.*, **193**(17-20), 1773-1788. https://doi.org/10.1016/j.cma.2003.12.025

Habibi, M., Mohammadi, A., Safarpour, H. and Ghadiri, M. (2021), "Effect of porosity on buckling and vibrational characteristics of the imperfect GPLRC composite nanoshell", *Mech. Based Des. Struct.*, **49**(6), 811-840. https://doi.org/10.1080/15397734.2019.1701490

Han, Y. and Elliott, J. (2007), "Molecular dynamics simulations of the elastic properties of polymer/carbon nanotube composites", *Comput. Mater. Sci.*, **39**(2), 315-323. https://doi.org/https://doi.org/10.1016/j.commatsci.2006.06.011

Jena, S.K., Chakraverty, S., Malikan, M. and Tornabene, F. (2020), "Effects of surface energy and surface residual stresses on vibro-thermal analysis of chiral, zigzag, and armchair types of SWCNTs using refined beam theory", *Mech. Based Des. Struct.*, 1-15. https://doi.org/10.1080/15397734.2020.1754239

Kachapi, S.H. (2020), "Surface/interface approach in pull-in instability and nonlinear vibration analysis of fluid-conveying piezoelectric nanosensor", *Mech. Based Des. Struct.*, 1-26. https://doi.org/10.1080/15397734.2020.1725566

Khadir, A.I., Daikh A.A, Eltaher, M.A., (2021), "Novel four-unknowns quasi 3D theory for bending, buckling and free vibration of functionally graded carbon nanotubes reinforced composite laminated nanoplates", *Adv. Nano Res.*, **11**(6), 621-640. https://doi.org/10.12989/anr.2021.11.6.621

Kolahdouzan, F., Mosayyebi, M., Ghasemi, F.A., Kolahchi, R. and Panah, S.R.M. (2020), "Free vibration and buckling analysis of elastically restrained FG-CNTRC sandwich annular nanoplates", *Adv. Nano Res.*, **9**(4), 237-250. https://doi.org/10.12989/anr.2020.9.4.237

Lim, C.W., Zhang, G. and Reddy, J. (2015), "A higher-order nonlocal elasticity and strain gradient theory and its applications in wave propagation", *J. Mech. Phys. Solids*, **78**, 298-313. https://doi.org/10.1016/j.jmps.2015.02.001

Lin, F. and Xiang, Y. (2014), "Vibration of carbon nanotube reinforced composite beams based on the first and third order beam theories", *Appl. Math. Modell.*, **38**(15-16), 3741-3754. https://doi.org/10.1016/j.apm.2014.02.008

Liu, H., Zhang, Q., Yang, X. and Ma, J. (2021), "Size-dependent vibration of laminated composite nanoplate with piezomagnetic face sheets", *Eng. Comput.*, 1-17. https://doi.org/10.1007/s00366-021-01285-y

Lu, L., She, G.L. and Guo, X. (2021), "Size-dependent post buckling analysis of graphene reinforced composite microtubes with geometrical imperfection", *Int. J. Mech. Sci.*, **199**, 106428. https://doi.org/10.1016/j.ijmecsci.2021.106428

Mahesh, V. and Harursampath, D. (2020), "Nonlinear deflection analysis of CNT/magneto-electro-elastic smart shells under multi-physics loading", *Mech. Adv. Mater. Struct.*, 1-25. https://doi.org/10.1080/15376494.2020.1805059

Matsunaga, H. (2008), "Free vibration and stability of functionally graded plates according to a 2-D higher-order deformation theory", *Compos. Struct.*, **82**(4), 499-512. https://doi.org/10.1016/j.compstruct.2007.01.030

Pham, Q.H., Nguyen, P.C., Tran, T.T. and Nguyen-Thoi, T. (2021), "Free vibration analysis of nanoplates with auxetic honeycomb core using a new third-order finite element method and nonlocal elasticity theory", *Eng. Comput.*, 1-19. https://doi.org/10.1007/s00366-021-01531-3

Qu, Y., Zhang, W., Peng, Z. and Meng, G. (2019), "Time-domain structural-acoustic analysis of composite plates subjected to moving dynamic loads", *Compos. Struct.*, **208**, 574-584. https://doi.org/10.1016/j.compstruct.2018.09.103

Radwan, A.F. and Sobhy, M. (2020), "Transient instability analysis of viscoelastic sandwich CNTs-reinforced microplates exposed to 2D magnetic field and hygrothermal conditions", *Compos. Struct.*, **245**, 112349. https://doi.org/10.1016/j.compstruct.2020.112349

Rai, A.K. and Gupta, S.S. (2021), "Nonlinear vibrations of a polar-orthotropic thin circular plate subjected to circularly moving point load", *Compos. Struct.*, **256**, 112953. https://doi.org/10.1016/j.compstruct.2020.112953

Reddy, J. (2007), "Nonlocal theories for bending, buckling and vibration of beams", *Int. J. Eng. Sci.*, **45**(2-8), 288-307. https://doi.org/10.1016/j.ijengsci.2007.04.004

Reddy, J.N. (1999), *Theory and Analysis of Laminated Composite Plates, In Mechanics of Composite Materials and Structures*, Springer, Dordrecht.

Roudbari, M.A., Jorshari, T.D., Arani, A.G., Lü, C. and Rabczuk, T. (2020), "Transient responses of two mutually interacting single-walled boron nitride nanotubes induced by a moving nanoparticle", *Eur. J. Mech. A Solids*, **82**, 103978. https://doi.org/10.1016/j.euromechsol.2020.103978

She, G.L. (2021), "Guided wave propagation of porous functionally graded plates: The effect of thermal loadings", *J. Therm. Stress.*, **44**(10), 1289-1305. https://doi.org/10.1080/01495739.2021.1974323

She, G.L., Liu, H.B. and Karami, B. (2021), "Resonance analysis of composite curved microbeams reinforced with graphene nanoplatelets", *Thin Wall. Struct.*, **160**, 107407. https://doi.org/10.1016/j.tws.2020.107407

Shen, H.S. (2009), "Nonlinear bending of functionally graded carbon nanotube-reinforced composite plates in thermal environments", *Compos. Struct.*, **9**1(1), 9-19. https://doi.org/10.1016/j.compstruct.2009.04.026

Shen, H.S. and Xiang, Y. (2012), "Nonlinear vibration of nanotube-reinforced composite cylindrical shells in thermal environments", *Comput. Meth. Appl. Mech. Eng.*, **213**, 196-205. https://doi.org/10.1016/j.cma.2011.11.025

Şimşek, M. (2010), "Dynamic analysis of an embedded

microbeam carrying a moving microparticle based on the modified couple stress theory", *Int. J. Eng. Sci*., **48**(12), 1721-1732. https://doi.org/10.1016/j.ijengsci.2010.09.027

Şimşek, M. and Aydın, M. (2017), "Size-dependent forced vibration of an imperfect functionally graded (FG) microplate with porosities subjected to a moving load using the modified couple stress theory", *Compos. Struct*., **160**, 408-421. https://doi.org/10.1016/j.compstruct.2016.10.034

Thai, H.T. and Choi, D.H. (2012), "A refined shear deformation theory for free vibration of functionally graded plates on elastic foundation", *Compos. Part B Eng*., **43**(5), 2335-2347. https://doi.org/10.1016/j.compositesb.2011.11.062

Wattanasakulpong, N. and Ungbhakorn, V. (2013), "Analytical solutions for bending, buckling and vibration responses of carbon nanotube-reinforced composite beams resting on elastic foundation", *Comput. Mater. Sci*., **71**, 201208. https://doi.org/10.1016/j.commatsci.2013.01.028

Zhang, L.H., Lai, S.K., Wang, C. and Yang, J. (2021), "DSC regularized Dirac-delta method for dynamic analysis of FG graphene platelet-reinforced porous beams on elastic foundation under a moving load", *Compos. Struct*., **255**, 112865. https://doi.org/10.1016/j.compstruct.2020.112865

Zhang, Y.Y., Wang, Y.X., Zhang, X., Shen, H.M. and She, G.L. (2021), "On snap-buckling of FG-CNTR curved nanobeams considering surface effects", *Steel Compos. Struct*, **38**(3), 293-304. http://dx.doi.org/10.12989/scs.2021.38.3.293

Zhu, P., Lei, Z.X. and Liew, K.M. (2012), "Static and free vibration analyses of carbon nanotube-reinforced composite plates using finite element method with first order shear deformation plate theory", *Compos. Struct*., **94**(4), 14501460. https://doi.org/10.1016/j.compstruct.2011.11.010

AT